

# On the finite element model updating of structural dynamics models

Über die Finite Elemente Modell-Updates von Strukturdynamik-Modellen

Semester Thesis

at the TUM School of Engineering and Design of the Technical University of Munich

**Supervisor** Prof. dr.ir. Daniel J. Rixen  
Chair of Applied Mechanics

**Advisor** Francesco Trainotti, M.Sc.  
Chair of Applied Mechanics

**Submitted by** Michael Bandara

**Submitted on** April 30, 2022 in Garching



## Abstract

There is a growing demand in industry for numerical finite element models capable of accurately and robustly predicting the behaviour of structural dynamic systems. This paper presents a workflow on the updating of such models, aiming to generate and optimise an FE model in Abaqus against measurements from experimental modal hammer testing, so that it may be considered representative of the real structure in question.

This paper addresses and quantifies errors that arise in doing so, such as any assumptions made during the creation of the model, spatial discretisation, measurement noise and accuracy and as to what degree these contribute on the desired dynamic behaviour. Damping forms an important, yet difficult factor of dynamic systems, specifically to both measure and conceptualise. As part of the model updating workflow, this paper explores various models of damping namely Rayleigh, structural and modal, each in their applicability and implementation for model updating.

The scope of the updating procedure is for the dynamic outputs of single, homogenous material structures over the frequency domain. It does not explore the extended topics involving contact/friction of assemblies and or time domain numerical models. Key takeaways are the understanding of the influence of experimental setup itself, a step by step workflow to update the models and their parameters, an overview of the assumptions involved and the overall applicability of the method.

## Zusammenfassung

In der Industrie gibt es eine wachsende Nachfrage nach numerischen Finite-Elemente-Modellen, die in der Lage sind, das Verhalten von dynamischen Struktursystemen genau und robust vorherzusagen. In diesem Beitrag wird ein Arbeitsablauf zur Aktualisierung solcher Modelle vorgestellt, der darauf abzielt, ein FE-Modell in Abaqus anhand von Messungen aus experimentellen modalen Hammertests zu erstellen und zu optimieren, so dass es als repräsentativ für die betreffende reale Struktur angesehen werden kann.

In diesem Beitrag werden die dabei auftretenden Fehler angesprochen und quantifiziert, wie z. B. die bei der Erstellung des Modells getroffenen Annahmen, die räumliche Diskretisierung, das Messrauschen und die Messgenauigkeit sowie die Frage, inwieweit sich diese auf das gewünschte dynamische Verhalten auswirken. Die Dämpfung ist ein wichtiger, aber schwieriger Faktor dynamischer Systeme, der sowohl gemessen als auch konzeptualisiert werden muss. Im Rahmen der Modellaktualisierung werden in dieser Arbeit verschiedene Dämpfungsmodelle untersucht, nämlich Rayleigh-, Struktur- und Modalmodelle, jeweils in ihrer Anwendbarkeit und Umsetzung für die Modellaktualisierung.

Der Anwendungsbereich des Aktualisierungsverfahrens bezieht sich auf die dynamischen Ergebnisse einzelner, homogener Materialstrukturen im Frequenzbereich. Es werden keine erweiterten Themen wie Kontakt/Reibung von Baugruppen oder numerische Modelle im Zeitbereich behandelt.

Die wichtigsten Erkenntnisse sind das Verständnis des Einflusses des Versuchsaufbaus selbst, ein schrittweiser Arbeitsablauf zur Aktualisierung der Modelle und ihrer Parameter, ein Überblick über die beteiligten Annahmen und die allgemeine Anwendbarkeit der Methode.

# Contents

- 1 Structural Dynamics Background** **1**
  - 1.1 Motivation . . . . . 1
  - 1.2 Finite Element Method in Structural Dynamics . . . . . 1
    - 1.2.1 Model Parameters . . . . . 2
    - 1.2.2 Damping . . . . . 2
    - 1.2.3 Dynamic Outputs . . . . . 3
  - 1.3 Model Updating . . . . . 5
    - 1.3.1 Sensitivity based optimisation . . . . . 5
  
- 2 Model Updating Procedure** **7**
  - 2.1 Step 1: Initial model . . . . . 7
  - 2.2 Step 2: Experimental Measurements . . . . . 8
    - 2.2.1 Weight measurement . . . . . 8
    - 2.2.2 Modal Hammer Testing . . . . . 9
  - 2.3 Step 3: Optimisation . . . . . 10
    - 2.3.1 Model Parameters . . . . . 10
    - 2.3.2 Damping . . . . . 11
  
- 3 Experimental Measurements** **13**
  - 3.1 Modal Hammer Testing . . . . . 13
  - 3.2 Test Setup . . . . . 13
    - 3.2.1 Boundary Conditions . . . . . 13
    - 3.2.2 Sensor Measurement . . . . . 14
    - 3.2.3 Impact testing procedure . . . . . 15
  
- 4 Results and Discussion** **17**
  - 4.1 Initial Models . . . . . 17
  - 4.2 Sensitivity Study . . . . . 17
    - 4.2.1 Mesh discretisation . . . . . 18
    - 4.2.2 Material Properties . . . . . 18
  - 4.3 Measurement Results . . . . . 20
    - 4.3.1 FRFs . . . . . 20
    - 4.3.2 Eigenfrequencies . . . . . 22
    - 4.3.3 Damping Ratios . . . . . 23
    - 4.3.4 Mode Shapes and MAC . . . . . 24
  - 4.4 Model Updating Case: A-Frame . . . . . 26
    - 4.4.1 Initial Model Results . . . . . 26
    - 4.4.2 Updated Density . . . . . 27
    - 4.4.3 Parameter Optimisation . . . . . 27
    - 4.4.4 Damping Comparison . . . . . 27
    - 4.4.5 Updated Model . . . . . 28

4.4.6	MAC	29
4.5	Model Updating Case: Beam	30
4.5.1	Initial Model Results	30
4.5.2	Updated Density	31
4.5.3	Parameter Optimisation	31
4.5.4	Damping Comparison	31
4.5.5	Updated Model	32
4.5.6	MAC	33
4.6	Discussion	34
4.6.1	Experimental MAC Discretisation	34
4.6.2	MAC - Experimental vs Numerical	35
4.6.3	Modes with close Eigenfrequencies	35
4.6.4	Beam - Structure Dimensions	36
4.6.5	Measurement errors and assumptions	37
4.6.6	Laser vs Accelerometer results	38
4.6.7	Invasive testing influence on eigenfrequency	39
4.6.8	Invasive testing influence on damping	41
4.6.9	Damping Scheme Comparison	42
4.6.10	Beam - Configuration comparison	44
4.6.11	Model Updating Effectiveness	45
<b>5</b>	<b>Conclusion</b>	<b>47</b>
5.1	Further exploration	48
<b>A</b>	<b>Appendix</b>	<b>49</b>
A.1	Beam Eigenmodes	49
A.2	A-Frame Eigenmodes	50
A.3	A-Frame MAC Table	51
A.4	Beam Configuration Positions	51

# Chapter 1

## Structural Dynamics Background

### 1.1 Motivation

Light weight structures have become more commonly found in products over time and also ever increasingly complex in design and shape due to developments in manufacturing. The ability of computers in numerical modeling has likewise progressed, with the increase in computing power and storage allowing for faster and more accurate models. [5]

More importantly however is the confidence in the models that they are able to be considered representative of the underlying system. Several parameters which go into modelling are fundamental in the behaviour of the system such as material properties, mesh discretisation, the damping scheme used. These parameters are often based on estimation, experience or resources on materials, however can present sources of error and inaccuracy as a result.

This motivates the identification of a robust and efficient workflow in a model updating procedure to identify, quantify and reduce such errors where possible. The scope of the use for the workflow is the identification of dynamic behaviour of single structures. Meaning the domain will only include the steady-state modal dynamics of single structures and not the topics of contact/friction relevant to assemblies and time integration for example.

### 1.2 Finite Element Method in Structural Dynamics

The use of finite elements refers to the discretisation of a continuous system into smaller "finite" elements, defining the interactions between them through dynamic system equations. This allows the continuous structure to then be formulated as individual degrees of freedom and the relationships between them formed into the newton equations based on the elements used and material properties. [4, 5]

As example these equations can be represented for a un-damped system in matrix-vector form below:

$$[M]\ddot{\mathbf{x}} + [K]\mathbf{x} = \mathbf{F} \quad (1.1)$$

Where  $[M]$  represents the mass matrix,  $[K]$  the stiffness matrix.  $\mathbf{x}$  and its double derivative  $\ddot{\mathbf{x}}$  represent vectors containing the displacement and acceleration of the  $N$  degrees of freedom respectively.  $\mathbf{F}$  is the vector of external force applied at the  $N$  degrees of freedom.

This can be extended to include damping depending on the scheme used (For this equation here we have viscous damping):

$$[M]\ddot{\mathbf{x}} + [C]\dot{\mathbf{x}} + [K]\mathbf{x} = \mathbf{F} \quad (1.2)$$

The finite element background and specific formulation of the mass and stiffness matrices for the relevant degrees of freedom based on element shape functions is beyond the scope of this paper and will not be explored in depth.

### 1.2.1 Model Parameters

In order to formulate a numerical model, properties of the structure must be used as inputs to the model. These properties will from here on be referred to as model parameters and make up the goal for the model updating procedure, in that they should be as close and representative of the real structure as possible.

Such model parameters include:

- **Structure Dimensions** The geometry of the continuous structure must be known and measured in order to define this volume within the numerical software.
- **Meshing** With a defined volume based on the structure's geometry, the next step is the spatial discretisation into finite elements. Of which there are several options and element types, the justification of the choices of the following parameters are well explored topics and present several guidelines to follow. As a general rule however the finer the discretisation, ie. smaller element sizes, the better approximation the numerical solution can provide.
- **Material properties** The parameters to provide most benefit from model updating, as they are difficult to be known to an accurate degree beforehand. No two structures are the same and sources of differences in such parameters arise from manufacturing processes.

### 1.2.2 Damping

Damping receives its own section here as is an important factor of the system that accounts for the energy loss of the system response due to dissipation or interactions through friction, heat, sound. [7] This however is a complicated topic, difficult to measure, conceptualise and implement accurately in a model. In any case, there are still several damping schemes that can be then implemented in the system to include this behaviour within a numerical model.

### Rayleigh Damping

The Rayleigh damping scheme implements a viscous damping matrix based on linear combinations of the mass and stiffness matrices [13]. Represented by the following equation:

$$[C] = \alpha[M] + \beta[K] \quad (1.3)$$

The parameters  $\alpha$  and  $\beta$  are scalar factors for each the mass and stiffness matrix respectively, the sum of the scaled matrices then compose the resulting viscous damping matrix.

### Structural Damping

Structural damping implements a damping force proportional to the stresses of the deformation. Unlike Rayleigh damping, the resulting damping forces are independant to the frequency of vibration. [10]

$$[M]\ddot{\mathbf{x}} + [K](1 + i\eta)\mathbf{x} = \mathbf{F} \quad (1.4)$$

The structural damping scheme is expressed in the equation above, where the term  $\eta$  is the damping loss factor.

### Modal Damping

Modal Damping is the scheme of applying individual damping ratios for each separate mode. This can be implemented where the dynamic system is expressed through modal superposition. In modal superposition the degrees of freedom of the system are then projected as the amplitudes of the relevant number of eigenmodes which the system has been projected onto. Where N number of eigenmodes are used, from the original N degree freedom system, the eigenmodes are able to span the basis of the original system. Since they are orthogonal, it is possible to then implement a viscous diagonal damping matrix, defining a specific damping ratio for each mode. [13]

## 1.2.3 Dynamic Outputs

### Eigenvalues and Eigenmodes

Once a system and each of its relevant model parameters are defined, the undamped natural frequencies can be identified through solving the non-trivial solution to the equation with no input force vector:

$$[M]\ddot{\mathbf{x}} + [K]\mathbf{x} = 0 \quad (1.5)$$

Which can be described as the solution where the inertial forces of the mass of the system during vibration are equally matched by elastic forces generated from the deformation during vibration. [13]

Reforming the equation into an eigenvalue problem allows the extraction of the natural frequencies in the form of eigenvalues and the relevant mode shapes as the corresponding eigenvectors.

$$[M]^{-1}[K]\mathbf{x} = \omega^2\mathbf{x} \quad (A\mathbf{x} = \lambda\mathbf{x}) \quad (1.6)$$

The damping matrix can also be included in the eigenvalue problem, where the solutions then become complex. Several approaches exist to solving these eigenvalue problems, most already implemented in commercial software as is the case in this paper where Abaqus is used.

### Modal Assurance Criterion - MAC

In order to quantify the correlation of eigenmode shapes the following formula is used for the MAC (Modal Assurance Criterion). This can be used to validate the eigenmode shapes determined experimentally against those obtained numerically. [1]

$$MAC(\{\psi_r\}, \{\psi_s\}) = \frac{|\{\psi_r\}^T \{\psi_s\}|^2}{\{\psi_r\}^T \{\psi_r\} \{\psi_s\}^T \{\psi_s\}} \quad (1.7)$$

As a further check, the MAC can be used to validate the orthogonality of eigenmode shapes. Where each eigenmode should have a value of 1 for perfect correlation to itself, as they are the same, and a correlation of 0 between any other different eigenmode.

### Damping Ratios

For lightly damped structures with well-spaced eigenfrequencies, it can be assumed there are effective damping ratios for each mode [13]. Starting with a damped system, the damping ratios can be obtained through solving the eigenvalue problem and using the modal mass and damping coefficients, or directly calculated from damping parameters depending on the scheme used (Rayleigh, Structural or Modal).

Alternatively they can sometimes use 3db method in obtaining damping ratios, directly measuring from an FRF (see following section). It does also assume however that contributions of each mode are able to be extracted from the FRF response itself, and again that the mode frequencies are well-spaced.

### Frequency Response Functions

Frequency response functions (FRF) represent the response of a structure for a specific output (Degree of freedom) over the frequency domain for a given input. It is obtained by taking the fourier transform of the output (whether it be in the units of acceleration, velocity or displacement) and divide by the fourier transform of the input, which is not necessarily the same position or degree of freedom.

This is the basis of the experimental modal impact testing component of the model updating procedure, as the eigenfrequencies and damping properties are to be experimentally obtained by analysis of the extracted FRF measured.

### Frequency Response Assurance Criterion - FRAC

Similarly to the MAC, the correlation of 2 FRF's can be investigated, in this case for validation of experimentally obtained FRFs against numerically obtained FRFs. Instead of vectors of coordinates however, it is the output response for a degree of freedom for a given input at another degree of freedom over the frequency domain. [1]

$$FRAC(\{H_r\}, \{H_s\}) = \frac{|\{H_r\}^T \{H_s\}|^2}{\{H_r\}^T \{H_r\} \{H_s\}^T \{H_s\}} \quad (1.8)$$

Similarly the correlation is then over the range between 0 (no correlation) and 1 (perfect correlation).

## 1.3 Model Updating

A model updating procedure has the goal to optimise a numerical model to be in agreement with a real structure based on the dynamic outputs measured through experiments. To do so there must be a quantifiable and relevant comparison of the defined dynamic outputs, where differences are then considered an error or cost function to be reduced.

There are 2 types of model updating, "Representational" (Direct) and "Knowledge-based" (Iterative). This paper presents purely the type involving knowledge-based due to its ability to preserve physical representation of the structure. Although Representational methods are able to perfectly update mass and stiffness matrices against experimental data in a direct, single step, they present the disadvantage of not guaranteeing the preservation of physical meaningfulness. [5]

Since numerical model parameters have varying effects on the dynamic outputs and are often non-linear in nature, for knowledge-based model updating, the optimized model must be obtained iteratively based on the objective function's sensitivity to the parameters. In addition it is important to be able to formulate the objective function used for optimisation, in such a way that presents a satisfactory and robustly approachable minimum. [13]

### 1.3.1 Sensitivity based optimisation

Sensitivity based methods iteratively update parameters based on the current error function's sensitivity (gradient) to the parameters. The error function is up to the user to be defined and is commonly referred to as the cost function. The idea being that if the processes are repeated until a criteria is met to define a minimum of the cost function, it has been optimised to where the error is smallest. [8]

Important is both a cost function and a gradient descent algorithm that enables good tracking over the cost function with each iteration and is able achieve a unique local minimum, which ideally is also the global minimum over the cost function domain.

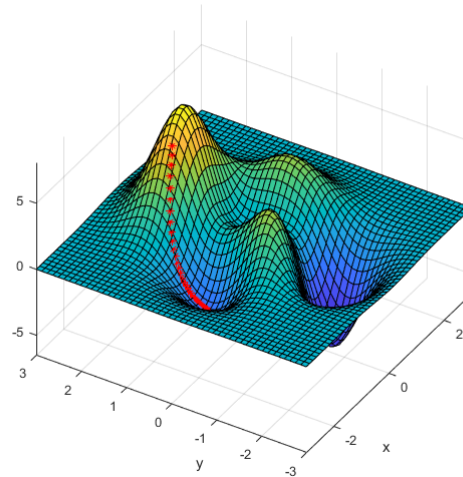


**Figure 1.1:** Gradient Descent Visualised.

Figure 1.1 graphically depicts the iterations of standard gradient descent with fixed learning rate over a 2 dimensional cost function surface. The red points represent the cost value  $Z$ , for a given combination of parameters  $X$  and  $Y$ . The initial cost is at the highest point and with each iteration it traverses the cost function surface in the direction of steepest gradient and updating  $X, Y$  values accordingly.

The local minimum which the algorithm here iterates to is shown - also visible is another local minimum which the algorithm may have iterated to had it different initial  $X, Y$  parameter values.

## Chapter 2

### Model Updating Procedure

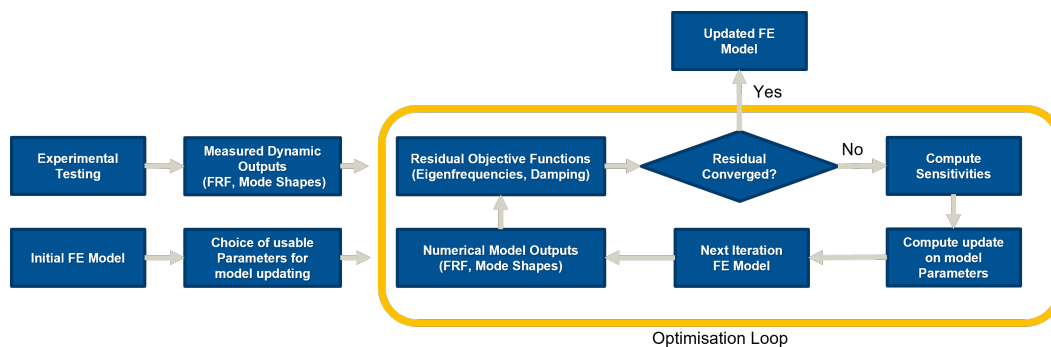


Figure 2.1: Model Updating Workflow.

In this chapter the defined and explored model updating procedure for the paper is described. The overall workflow is illustrated above.

#### 2.1 Step 1: Initial model

To begin, an initial FE model is needed to be created to base the updating procedure on. This initial model is not just important to gain a first impression of the structure, but it is also important before modal impact testing is carried out. A requirement for modal impact testing is that the points at which to impact the structure, exciting the relevant eigenmodes so that they may be identified, (Controllability). In addition that the points of measurements are able to then capture the relevant excited eigenmodes (Observability). [13]

An initial FE model with reasonable geometry and some baseline model parameters, can still be used for eigenmode extraction numerically. This allows to make beforehand an identification of useful points for the modal hammer testing.

For a given geometry of the structure, there are several well-explored and commonly agreed upon meshing guidelines to follow [2]. These are implemented in obtaining the initial model. Such guidelines for example:

- Have at least 3 elements across any width of the structure cross section
- No elements having a significantly distorted shape (aspect ratio)
- Consistent and smooth mesh that encompasses the shape of the geometric structure

For parts of a structure with thin cross sections that approach planar geometry, 2D shell elements could be more applicable than 3D elements such as the tetra/hexahedron. That can however come with more complications in the appropriate way of modelling such elements where the geometry is complex. In this paper there is no such example used.

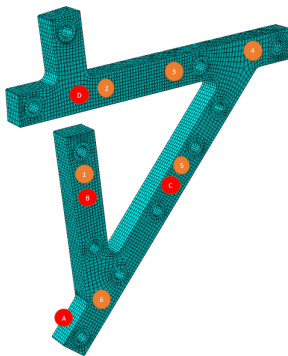


**Figure 2.2:** A-Frame Structure.

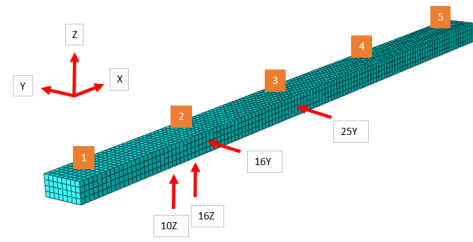


**Figure 2.3:** Beam Structure.

Here the figure 2.2 shows the strike points (red) and the measurement points (orange) which have been identified for the A-Frame to both excite and measure the eigenmodes. Figure 2.3 shows the beam structure and 4 strike points (red) identified. The 5 points of measurement (orange) are along the top face of the beam equally spaced.

Together these points are then used for both impact and measurement points in the following experimental modal impact testing step. The orange points in both figures are locations for the numerical model to have point masses added, representing added mass of the accelerometers.

## 2.2 Step 2: Experimental Measurements

### 2.2.1 Weight measurement

The second step involves first measuring the weight of the structure, which may or may not there itself present issues. If the assumption that the structure in question has a homogenous material, density can be calculated if the mass and geometry are both known. For the use cases of this model updating workflow, the structures are assumed to be known as homogenous material and measurement of the structure weight is feasible.

As a general rule, the amount of mass and stiffness have opposing effects on the frequency response of dynamic systems. Meaning a consistent increase in mass or a decrease in stiffness will both cause a reduction in the resonance frequencies [13]. This is the reason the measurement of weight in step 2 is important, because to include density as part of the gradient

descent optimisation step, will cause issues since there are many combinations of density and Youngs modulus that will iterate to a minimum.

With density then as a known and calculated input parameter, it leaves the Youngs modulus and Poisson ratio the two remaining parameters to optimise for against eigenfrequency error and generally have a better defined cost function surface in terms of iterating to a minimum.

In addition the mass of the accelerometers are important to measure and include in the model as they are attached and become part of the system being measured. They have been seen to influence the outputs of the system, see discussion section. In this workflow they are implemented as point masses.

### 2.2.2 Modal Hammer Testing

The purpose of modal hammer testing as part of the work flow is to obtain reference dynamic outputs of the structure. Specifically, the outputs for the previously identified input points. Having then obtained the FRFs of the real structure, the eigenfrequencies are able to be identified where peaks in the response occur for a given frequency.

Damping is also able to be approximated through a single or multi-DoF identification techniques such as the half-power method where modes are well spaced. In this paper, the Siemens LMS software is used, which utilizes Polymax multi-reference modal identification in extracting the frequency and damping values from the FRF.

To illustrate the steps, figure 2.4 shows the modal hammer used to strike the points identified by the red arrows in figure 2.5.



**Figure 2.4:** Modal Hammer.

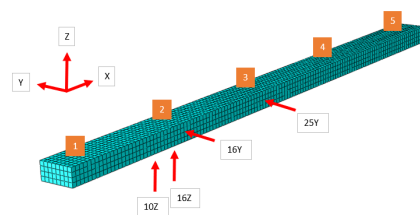


**Figure 2.5:** Beam Strike Points.

The resulting output (through the Siemens LMS software) are the accelerations shown in the following figure 2.6 as an example of the acceleration response at the orange position 1 in the Y-direction in figure 2.5.

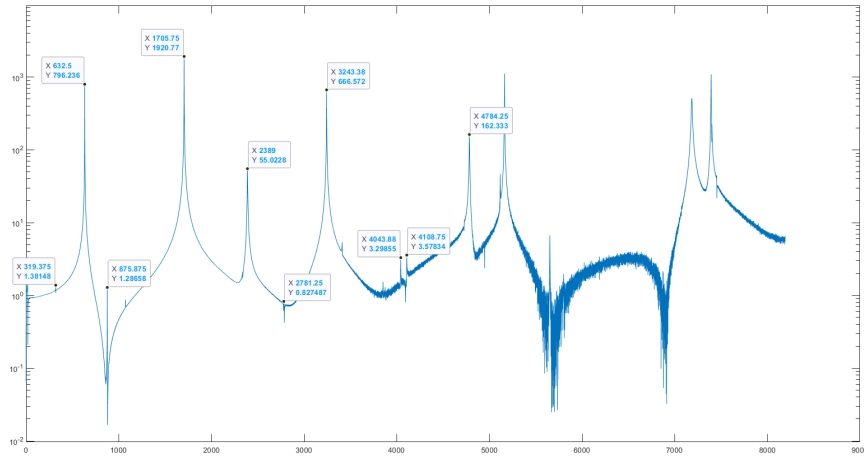


Figure 2.6: FRF - Strikepoint 16Y.

## 2.3 Step 3: Optimisation

### 2.3.1 Model Parameters

The optimisation of the model parameters relevant to the natural eigenfrequencies in this paper utilise sensitivity based methods, meaning the relevant outputs of the model must be sensitive to the parameters chosen. Specifically here the "nonlinsq" option in the Matlab optimisation toolbox is implemented with the Levenbourg-Marquardt algorithm. It provided the best tracking to a local minimum in terms of step progression and total time taken, however other options are available. [6, 11]

The initial model has starting parameter values taken from within an expected value range given from a material handbook [3]. The cost function for the "nonlinsq" optimisation is here defined through the squared percentage difference of the natural eigenfrequencies. Rather than the error magnitudes themselves (deltas), here the percentage differences are used to account for the different magnitudes of the frequencies. This would otherwise weight the higher frequencies more than the lower frequencies.

Mode	Initial	Measurements	Delta	%
1	322.70	319.42	3.28	1.03%
2	636.71	632.41	4.30	0.68%
3	884.80	875.67	9.13	1.04%
4	1716.60	1703.15	13.45	0.79%
5	1720.74	1705.69	15.05	0.88%
6	2416.28	2389.17	27.11	1.13%
7	2814.45	2785.91	28.54	1.02%
8	3263.80	3243.50	20.30	0.63%
9	4150.06	4107.72	42.34	1.03%
10	4835.77	4784.18	51.59	1.08%

Table 2.1: Example Eigenfrequency Comparison - Initial vs Experimental

In addition the square percentage differences for each mode are applied with weighting function to them that is inversely proportional to their eigenfrequency. This is to account for both the higher confidence and relevance in the measurement of lower frequency modes. Higher frequency responses exhibited more noise and are less capable of accurate results from measurement equipment and therefore have less confidence in their values.

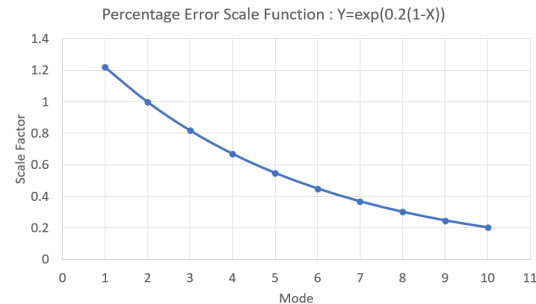


**Figure 2.7:** Error Scale Function Per Mode.

### 2.3.2 Damping

For this paper, the structures and their material composition together have very low damping (<1%), this allows the assumption that the natural eigenfrequencies are very close in value to the damped eigenfrequencies. [9]

Using the assumption above, the damping characteristics do not need to be included as model parameters during optimisation. A direct least squares approach is then implemented with the experimentally obtained modal damping ratios to calculate optimal damping parameters depending on the scheme of Rayleigh or Structural.



## Chapter 3

# Experimental Measurements

Here the experimental procedure is outlined, detailing the experimental setup and equipment used.

### 3.1 Modal Hammer Testing

Modal hammer testing involves striking a structure with a hammer with a specialized piezoelectric tip that generates an impulse force signal with frequency content that covers the range of eigenfrequencies of interest within the structure [14]. The signal of force applied on the structure, measured within the hammer's tip is recorded over time, while the resulting response of the structure is measured through either accelerometers (more invasive) or through laser equipment (non-invasive). The experimental measurements were using the Siemens LMS Testlab modal impact testing equipment and software.

### 3.2 Test Setup

The experimental setup was chosen to best allow the extraction of the dynamic outputs of the structure itself. The goal is to be as least-invasive as possible and to not have additional effects on the dynamic outputs as a result of taking the measurements themselves. Factors such as additional mass from attachments and signal cables attached to sensors and the structure can have a significant effect in the dynamic outputs that are measured. They can also come from the boundary conditions in place for the test.

The use of a laser requires no added mass (less invasive) however is only able to measure in a single direction. The laser allows comparison between the measurements obtained with and without the accelerometer to isolate its affect on the system.

#### 3.2.1 Boundary Conditions

The boundary conditions used for the modal hammer testing are aimed to be free-free, to excluding complex interaction such as contact/friction/pre-tension from any kind of fixation. This is possible in the numerical model in Abaqus, however experimentally there must be some fixation to suspend the structure while affecting it as little as possible. The fixation implemented for this test was to suspend structure with fishing wire as this has very little

contact area on the structure, while also little constraint in the rigid body movements, excepting tension along the direction of the wire.

### 3.2.2 Sensor Measurement



**Figure 3.1:** Laser Measurement Device.

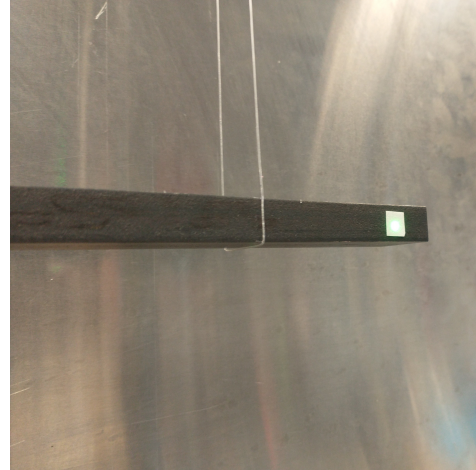


**Figure 3.2:** Laser Measurement Position.

In figures 3.1 and 3.2 the setup shown is for the laser only measurement, where the response is measured through a laser being projected onto the structure and reflected off, re-captured by the same equipment. This allows a calculation of velocity of the point of contact, representing the structures output in velocity for the given force input.

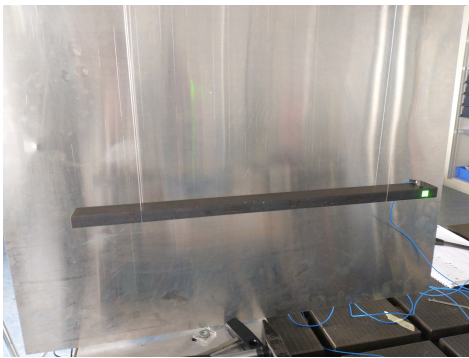


**Figure 3.3:** Laser With Accelerometer Setup.

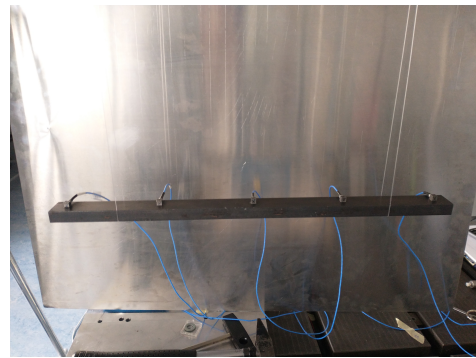


**Figure 3.4:** 5 Accelerometer Setup.

Similarly in figures 3.3 and 3.4 we see the setup where accelerometers are now included for the beam structure, these measure accelerations in 3 components (X,Y and Z) of its own reference system. They have been attached directly to the structure with a strong adhesive glue.

The following figures 3.5 and 3.6 show the less invasive (2 Accelerometers) and more invasive (6 Accelerometers) setups for the A-Frame structure respectively.

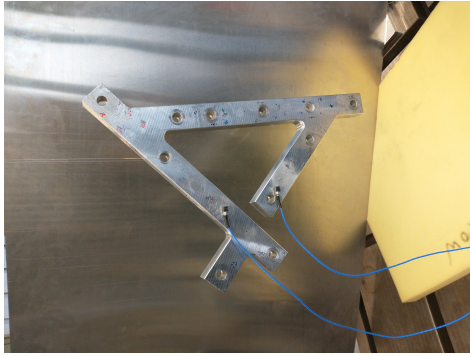


**Figure 3.5:** A-Frame with 2 Accelerometers.

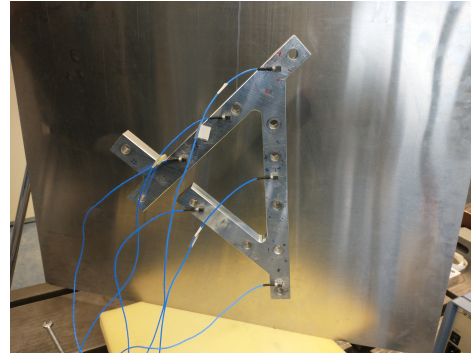


**Figure 3.6:** A-Frame with 6 Accelerometers.

The choice of location for measurements to be taken are also based on the initial model results, in that it can be identified which combination of points should exhibit most deformations for the measurable eigenmodes (Observability) [13].

### 3.2.3 Impact testing procedure

As explained in the previous chapter, an initial FE model can allow the user to identify where key points are needed to be struck with the modal hammer and equally important where the response is to be measured. This has been used prior to the impact testing procedure, the specific locations for striking to excite the eigenmodes are determined. There is likely not one single location that will experience deformation over all eigenmodes, hence the initial model is important to see which minimal set of points can be tested while obtaining a response from the eigenmodes of interest. [12]



**Figure 3.7:** Modal Hammer.

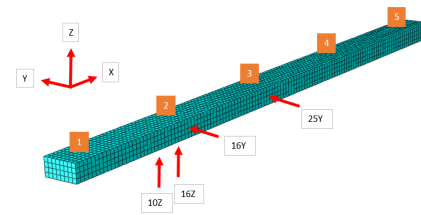


**Figure 3.8:** Beam Strike Points.

Figure 3.7 above shows the modal hammer used for the experimental impact testing, while figure 3.8 shows the identified strike points for the beam and the reference system they belong to. The second eigenmode of the beam structure from the initial model is visible in Figure 3.9. Together figure 3.8 and 3.9 highlight the contribution of this mode shape for the strike point "25Y" as example where there is deformation present at this location in this degree of freedom.

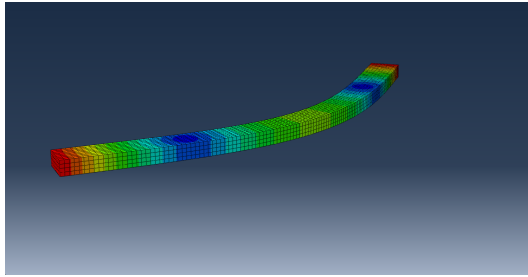


**Figure 3.9:** Beam 2nd Eigenmode.

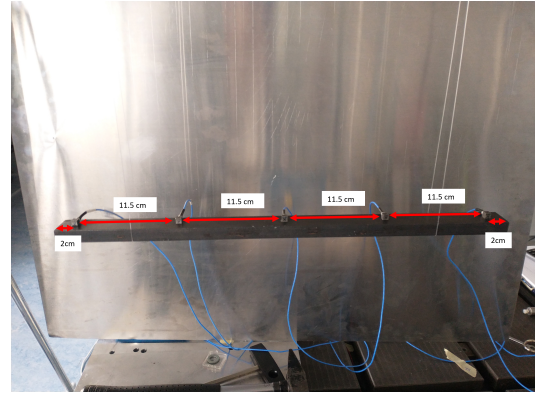


**Figure 3.10:** Beam 5 Accelerometer Positions.

Furthermore figure 3.9 shows the attachment of the 5 accelerometers for the more-invasive configuration. This setup with more positions and degrees of freedom measured, allows the better extraction of the eigenmode shapes given its better observability of the overall structure deformation. The mode shapes are then extracted from the structure through the Siemens LMS software. While we expect slightly different dynamic response of the system from the additional masses, assuming well separated eigenfrequencies, we are able to match and confirm the correct eigenmodes obtained from the numerical model.

Figure 3.11 below shows the experimentally obtained 2nd eigenmode of the beam structure. Good correlation with the numerically obtained 2nd eigenmode is visible when compared to figure 3.9. It must be understood the eigenmode shapes are equal with only different magnitudes and as a result appears different.

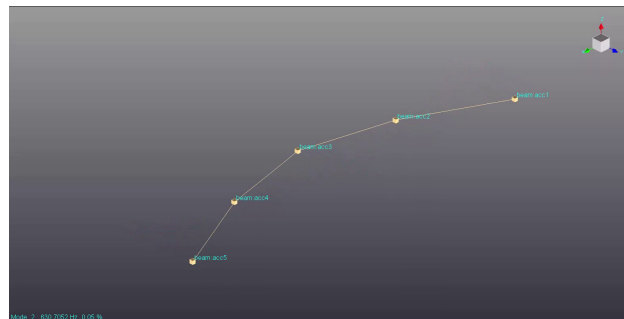


**Figure 3.11:** Beam 2nd Eigenmode - Experimentally obtained.

# Chapter 4

## Results and Discussion

### 4.1 Initial Models

The following properties and values are used in the initial models for the Beam and A-Frame structures. These values are based for standard references for Steel and Aluminium materials. [3]

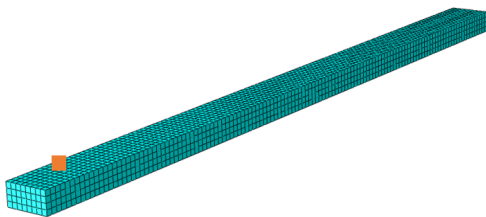


Figure 4.1: Mesh Beam Structure

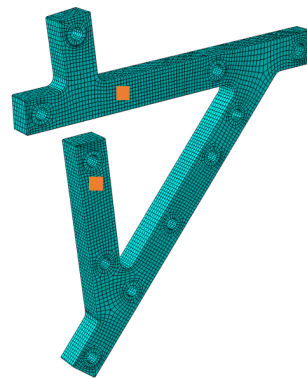


Figure 4.2: Mesh A-Frame Structure

Beam:

Material - Steel

Youngs Modulus: 210 GPa

Poisson Ratio: 0.27

Density: 7800 kg/m<sup>3</sup>

A - Frame:

Material - Aluminium

Youngs Modulus: 70 GPa

Poisson Ratio: 0.32

Density: 2700 kg/m<sup>3</sup>

To represent the addition mass from accelerometers in the less-invasive configurations, point masses of 2.3 grams are added at the orange positions in figures 4.1 and 4.2. These are kept constant for the model.

### 4.2 Sensitivity Study

To understand the effect each parameter has on the dynamic outputs of the system a sensitivity study is performed. Through variation of the parameters by small percentages (within reasonable tolerances), the resulting affect in the relevant outputs can be observed and better understood. It also forms the basis for the sensitivity based iterative methods in approximating derivative values.

### 4.2.1 Mesh discretisation

Meshing of the structure describes the spatial discretisation of the continuous structure. As a result the finer the elements, the closer the model will represent the real structure. However this comes at a cost of the computations required in terms of larger amount of degrees of freedom. The graph below presents the changes in the eigenfrequencies as a function of mesh seed sizes, from 7mm down to 2mm with 1mm increments each relative to the 1mm seed size.

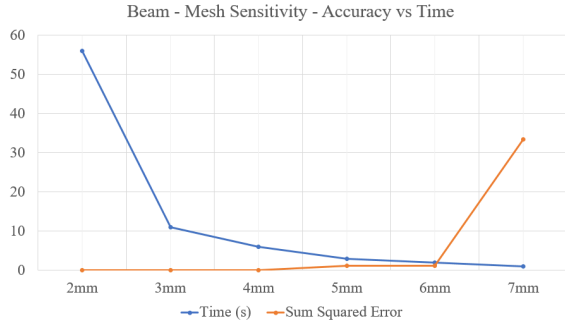


Figure 4.3: Beam Mesh Sensitivity Study

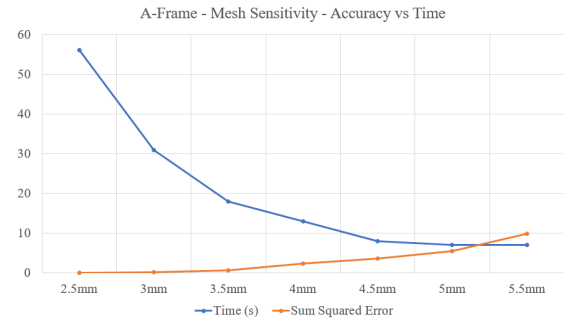


Figure 4.4: A-Frame Mesh Sensitivity Study

As a result of the mesh sensitivity investigation, the mesh element size was chosen as 4mm for both a trade-off in accuracy and computation time. The time of 6s is reasonable while still maintaining large proportion of accuracy with respect to mm mesh eigenfrequencies.

### 4.2.2 Material Properties

Youngs modulus and Density values are varied by +/- 0.5 and 1.0 percent respectively from the initial model values. These variations are chosen to keep within a reasonable range of the values for the material Steel. [3]

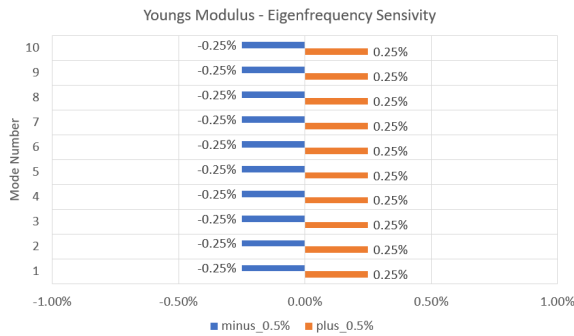


Figure 4.5: Sensitivity Youngs Modulus

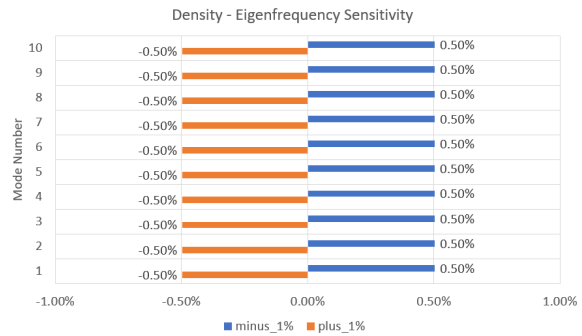
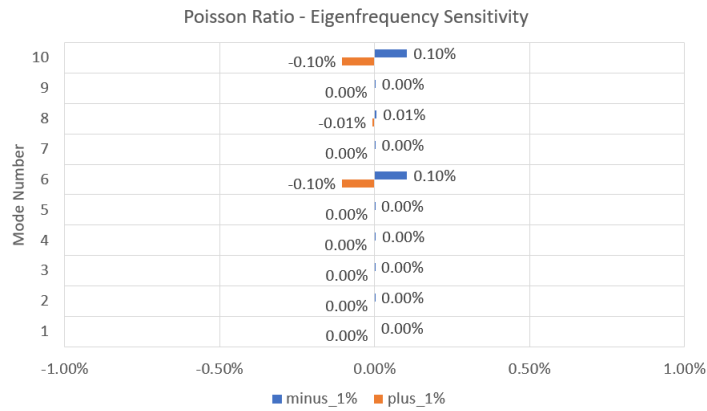


Figure 4.6: Sensitivity Density

Youngs Modulus and Density show consistent effect on all eigenfrequencies as expected due to their inherent behaviour as constant factors within both the stiffness and mass matrices respectively. This highlighting the necessity for the density to be initially solved for through weight measurement, otherwise there is a pairwise solution to finding minimum based on least square errors of eigenfrequencies with some combination of Youngs modulus and density.

The Poisson ratio also has some variability for different materials and so is also investigated as part of the sensitivity study.



**Figure 4.7:** Sensitivity Poisson Ratio

Poisson ratio however is almost exclusively having influence on their eigenmodes 6 and 10, both of which are the only "torsional" modes within the first 10 eigenmodes. This could be expected since the Poisson ratio is a factor affecting the coupling of axial and shear strain within elements, which the deformation within the torsional modes exhibit more of.

### 4.3 Measurement Results

#### 4.3.1 FRFs

The following FRFs illustrate the relevant response of the beam structure and how they are dependant on the impact position and direction into the system. Figure 4.8 shows the 4 different striking positions and their respective directions on the beam structure.

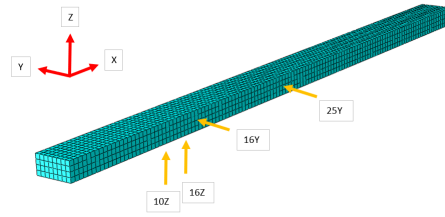


Figure 4.8: Beam Strike Points

Figure 4.9 below corresponds to the FRF with the modal hammer striking in the position and direction 16Y in configuration 1. The direction of force corresponds to the eigenmodes that have largest deformation in the same plane XY.

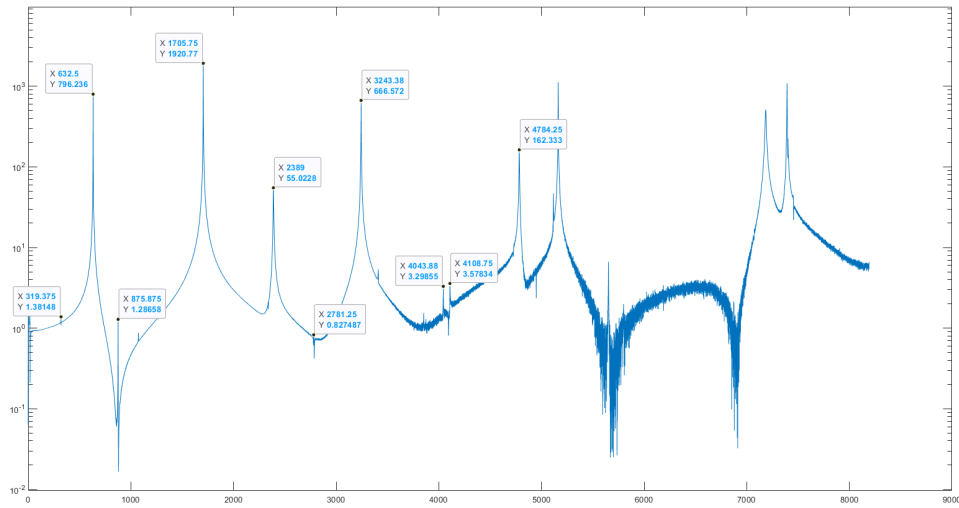


Figure 4.9: Beam FRF Strike Point 16Y

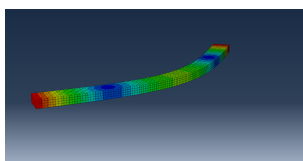


Figure 4.10: Mode 2 - 632.5 Hz

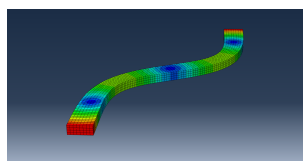


Figure 4.11: Mode 5 - 1705.75 Hz

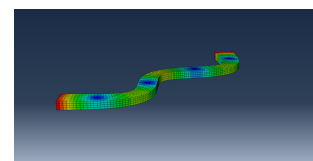
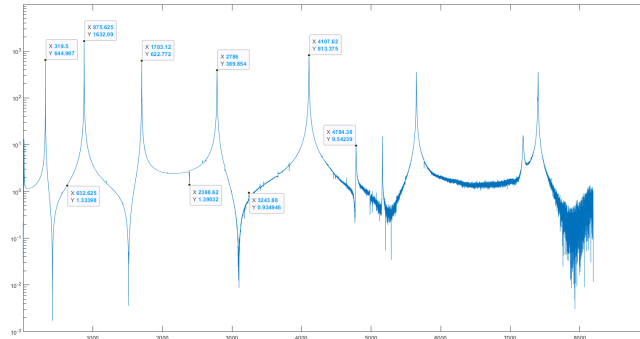
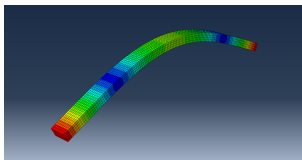


Figure 4.12: Mode 8 - 2389 Hz

The first 3 peaks from figure 4.9 are represented by the 3 eigenmodes visualised from figures 4.10,4.11 and 4.12. The clear correlation between the eigenmodes in the XY plane, and the strike position is presented.



**Figure 4.13:** Beam FRF Strike Point 16Z



**Figure 4.14:** Mode 1 - 319.5 Hz

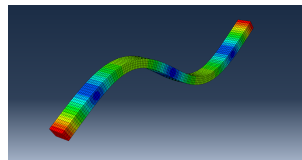


**Figure 4.15:** Mode 3 - 875.625 Hz

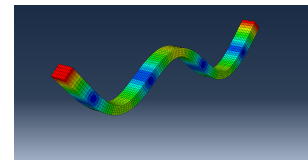


**Figure 4.16:** Mode 4 - 1703.12 Hz

Similarly when the FRF for the strike position and direction 16Z, we observe peaks in figure 4.13 now at the frequencies relevant to the eigenmodes with deformation in the plane YZ. The first 3 peaks of the FRF represent the eigenmodes shown in figures 4.14, 4.15 and 4.16.

The 2 FRFs are shown here to illustrate the response of the structure for a given impact and the importance of the initial model beforehand to identify strike positions that are able to excite the relevant modes. It should however be mentioned that despite the impact being aimed in single directions against the beam faces, it is never quite perfect in direction or position. In addition, the structure is also not perfectly symmetric even with its material throughout. As a result it, even out of plane eigenmodes are somewhat excited when struck in a position and direction that it does not correspond to. This is visible by the significantly smaller yet still present peaks at these frequencies.

For the case of the beam, the paper explores and includes up to the first 10 eigenmodes of the structure for updating, 8 of which lie exclusive within individual planes, the remaining 2 are torsional modes. These torsional modes can be seen in Appendix A1. The A-Frame is a more complex structure, in this case the first 15 eigenmodes are used for the modal updating.

For the final comparison purposes, the sum of the FRFs for each strike position are used, with the goal to provide cleaner comparisons between different the FRFs. Otherwise as visible in figures 4.9 and 4.13 there are anti-resonants and noise that make up larger and more difficult to match proportions within FRAC comparisons. The summed FRFs preserve the most relevant dynamic outputs, being eigenfrequencies and damping ratios.

### 4.3.2 Eigenfrequencies

Mode	Laser	1 Acc	5 Acc
1	319.74	319.40	318.88
2	633.49	632.48	630.87
3	876.42	875.79	874.24
4	1703.92	1702.99	1699.38
5	1707.43	1705.82	1701.00
6	2389.17	2389.37	2383.87
7	2786.86	2785.71	2784.16
8	3244.90	3243.53	3231.20
9	4109.26	4108.00	4101.74
10	N/A	4784.49	4775.06

**Table 4.1:** Eigenfrequencies - Beam

The eigenfrequencies obtained experimentally from the Polymax method in Siemens LMS are shown for each of the different test setups. Represented in the results is the almost consistent decrease in frequencies with the addition of masses from 1 accelerometer and more so with 5 accelerometers. It is almost consistent because for the 6th mode, there is actually a very minor increase in the frequency from the laser to using one accelerometer. The likely small magnitude is a result of the additional mass having small/no effect on the eigenmode, meaning its location being at a zero.

However it even increases, theoretically this should not occur, however given the small magnitude of difference, its increase could be attributed to noise in the FRF and error introduced as a result within the eigenfrequency extraction in the LMS software. The 10th eigenmode was also not visible in the FRF generated from the laser. The higher frequencies had significant noise relative to the lower frequencies (See earlier figure 4.9 for example).

Mode	2 Acc	6 Acc
1	282.23	281.99
2	310.49	309.76
3	624.78	622.61
4	717.36	716.27
5	1089.01	1087.10
6	1252.54	1248.47
7	1698.70	1692.91
8	2269.02	2263.58
9	2308.68	2302.57
10	2380.50	2372.40
11	3111.12	3103.01
12	3642.74	3636.23
13	4048.08	4033.11
14	4389.76	4375.02
15	4559.54	4555.54

**Table 4.2:** Eigenfrequencies - A Frame

Similar trend is seen for the A Frame structure, with the frequencies consistently decreasing with the change of 2 accelerometers to 6. The laser was not used for the A-Frame.

### 4.3.3 Damping Ratios

Mode	Laser	1 Acc	5 Acc
1	0.027%	0.042%	0.072%
2	0.017%	0.033%	0.063%
3	0.016%	0.024%	0.034%
4	0.012%	0.018%	0.038%
5	0.010%	0.023%	0.042%
6	0.012%	0.047%	0.086%
7	0.015%	0.020%	0.030%
8	0.009%	0.024%	0.127%
9	0.021%	0.020%	0.029%
10	N/A	0.041%	0.124%

**Table 4.3:** Damping Ratios - Beam

Similarly the experimental damping ratios are obtained through the Polymax method in the Siemens LMS Software. Similarly to the effects on eigenfrequencies, we see clear increase in the damping ratios obtained where the accelerometers are implemented in measurements for the beam structure. However this cannot simply be attributed to the additional mass from the accelerometers.

A reasonable explanation of the consistent increase in damping ratio values obtained with more accelerometers attached, is being due to energy transfer during resonance from the structure through the wires attached to the accelerometers.

Again we observe consistent increase in damping ratios for the A-Frame structure in table 4.4 below.

Mode	Acc 2	Acc 6
1	0.067%	0.076%
2	0.011%	0.030%
3	0.004%	0.058%
4	0.078%	0.106%
5	0.006%	0.017%
6	0.008%	0.037%
7	0.007%	0.048%
8	0.021%	0.062%
9	0.015%	0.036%
10	0.037%	0.111%
11	0.047%	0.059%
12	0.040%	0.154%
13	0.035%	0.080%
14	0.014%	0.092%
15	0.133%	0.154%

**Table 4.4:** Damping Ratios - A Frame

#### 4.3.4 Mode Shapes and MAC

Mode shapes were obtained experimentally through the use of 5 and 6 accelerometers for the Beam and A-Frame respectively (most-invasive setups). The setups are shown in figures 4.17 and 4.18.

The mode shapes are reconstructed using the Siemens LMS Software at the coordinates of the accelerometers for each eigenmode. For illustration, the reconstructed first eigenmode for each structure are visually presented in figures 4.19 and 4.20. The eigenmode shapes linearly interpolated between the displacements at the points generated at the accelerometer locations.

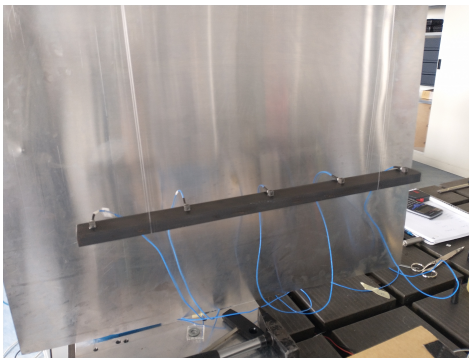


**Figure 4.17:** Beam 5 Accelerometer Setup

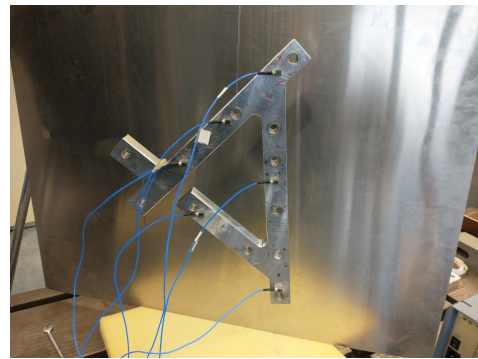


**Figure 4.18:** A-Frame 6 Accelerometer Setup

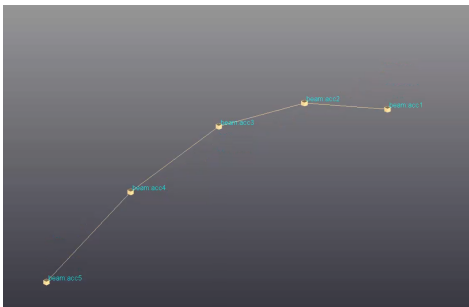


**Figure 4.19:** Extracted 1st Eigenmode - Beam

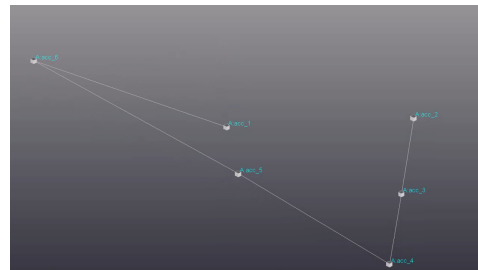


**Figure 4.20:** Extracted 1st Eigenmode A-Frame

A tool to validate the experimentally obtained eigenmode shapes is the MAC, and compare all permutations of the measured mode shapes. This is to check whether the eigenmodes obtained from the results preserve the requirement of orthogonality between them.

Ideally the MAC criterion uses all degrees of freedom, however due to limitations of measurement positions and accelerometers only those shown in the figures here are used in the MAC computation, making this an incomplete MAC comparison.

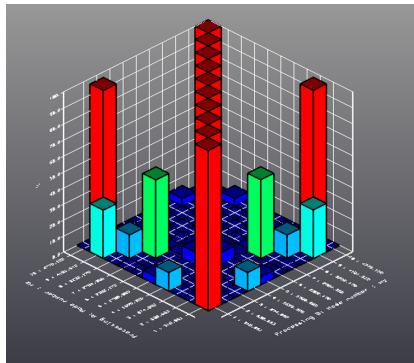


Figure 4.21: Experimental MAC : Beam

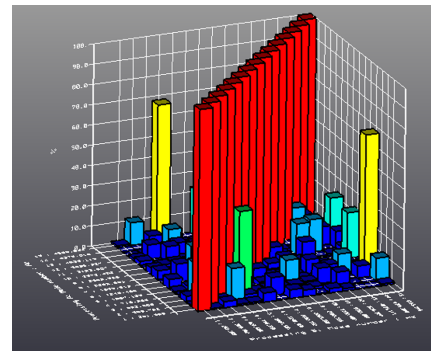


Figure 4.22: Experimental MAC : A-Frame

The MAC criterion for each structure is shown above, figure 4.21 for the Beam structure and figure 4.22 for the A-Frame. In each figure, the diagonal values represent the correlation with each eigenmode and itself (1.0 perfect correlation). For eigenmodes to be orthogonal they must have 0 correlation with any eigenmode other than itself.

For both structures tested however, we see there exists some correlation between different eigenmodes. This could be attributed to inaccuracy in the measurements ie. positions and orientations of the sensors however it is likely a result of the insufficient number of points and degrees of freedom measured.

The values of the MAC for the experimentally obtained eigenmodes for the beam are presented in table 4.5 below as percentages up to the first 10 eigenmodes.

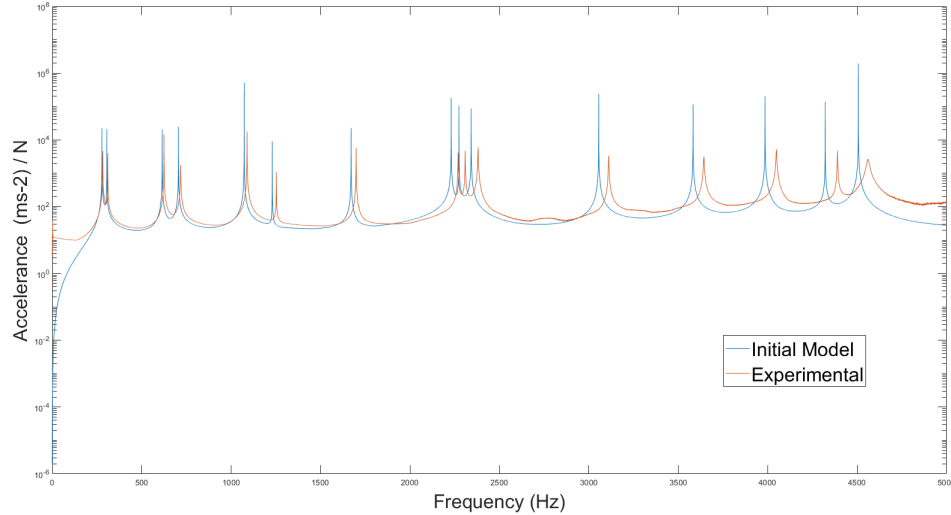
	1	2	3	4	5	6	7	8	9	10
1	100.0	0.0	0.0	11.7	5.0	0.1	0.2	0.0	30.2	0.1
2	0.0	100.0	0.0	0.0	0.0	0.1	0.0	14.7	0.0	96.8
3	0.0	0.0	100.0	0.1	0.1	0.1	49.1	0.0	0.4	0.0
4	11.7	0.0	0.1	100.0	7.9	1.8	0.5	0.0	3.7	0.0
5	5.0	0.0	0.1	7.9	100.0	3.2	0.3	0.1	1.8	0.0
6	0.1	0.1	0.1	1.8	3.2	100.0	0.1	0.0	0.0	0.1
7	0.2	0.0	49.1	0.5	0.3	0.1	100.0	0.0	0.0	0.0
8	0.0	14.7	0.0	0.0	0.1	0.0	0.0	100.0	0.0	4.8
9	30.2	0.0	0.4	3.7	1.8	0.0	0.0	0.0	100.0	0.2
10	0.1	96.8	0.0	0.0	0.0	0.1	0.0	4.8	0.2	100.0

Table 4.5: Experimental MAC Numerical Values : Beam

The table for the A frame can be found in the Appendix A.3, as it is too large to present here.

## 4.4 Model Updating Case: A-Frame

### 4.4.1 Initial Model Results



**Figure 4.23:** A-Frame SUM FRF : Initial vs Experimental

Figure 4.23 overlays the experimentally obtained sum of FRFs with the numerically obtained sum of the FRFs of the initial model of the A-Frame. The reference values used are from the less-invasive test configuration (2 accelerometers) as this had the best clarity for measurements. There is loss in correlation relating to the exclusion of both boundary conditions and rigid body modes in the numerical model. With all input projected onto the first 10 eigenmodes, there is no response as the input approaches 0 Hz in frequency. Through use of the FRAC as a measurement of correlation it has a value of 0.9391.

Mode	Initial	Measurements	Delta	%
1	277.95	282.23	-4.28	-1.51%
2	305.27	310.49	-5.22	-1.68%
3	614.83	624.78	-9.95	-1.59%
4	705.46	717.36	-11.90	-1.66%
5	1073.00	1089.01	-16.01	-1.47%
6	1230.11	1252.54	-22.43	-1.79%
7	1670.71	1698.70	-27.99	-1.65%
8	2230.10	2269.02	-38.92	-1.72%
9	2274.02	2308.68	-34.66	-1.50%
10	2341.96	2380.50	-38.54	-1.62%
11	3055.36	3111.12	-55.76	-1.79%
12	3582.59	3642.74	-60.15	-1.65%
13	3985.09	4048.08	-62.99	-1.56%
14	4321.61	4389.76	-68.15	-1.55%
15	4506.63	4559.54	-52.91	-1.16%

**Table 4.6:** Initial vs Experimental Eigenfrequencies : A-Frame

Table 4.6 shows a comparison of eigenfrequencies between the initial model and the ex-

perimental measurements. The mean square error of the eigenfrequencies for the initial model against the experimental is 155.46. The range of percentage errors is consistent between -1.16% to -1.79%. Likely indicating a lack of stiffness or lower Youngs modulus value, or alternatively a surplus of mass and a higher density value needed to represent the structure.

#### 4.4.2 Updated Density

With a weight measurement of the beam at 1.268kg, for the given dimensions the density is then calculated to be 2661 kg/m<sup>3</sup>.

Initial Density: 2700kg/m<sup>3</sup> -> 2661 kg/m<sup>3</sup> Updated

#### 4.4.3 Parameter Optimisation

After the Optimisation steps, we obtain the following updated parameters:

Initial Youngs Modulus: 70,000 MPa -> 71,352 MPA Updated

Initial Poisson Ratio: 0.32 -> 0.32671 Updated

#### 4.4.4 Damping Comparison

Rayleigh damping was implemented with values calculated through a least squares approach against the experimentally obtained damping ratios per mode. The obtained  $\alpha$  and  $\beta$  parameters were:

$$\alpha = 1.3438$$

$$\beta = 3.7917E^{-8}$$

The effective damping ratio per mode is plotted in figure 4.24 below, showing the difference between Rayleigh damping scheme the measured damping ratios.

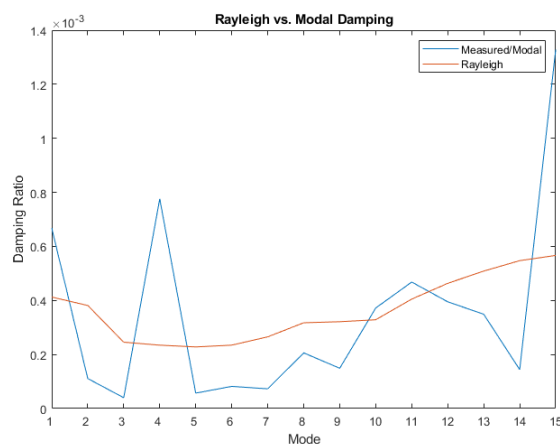
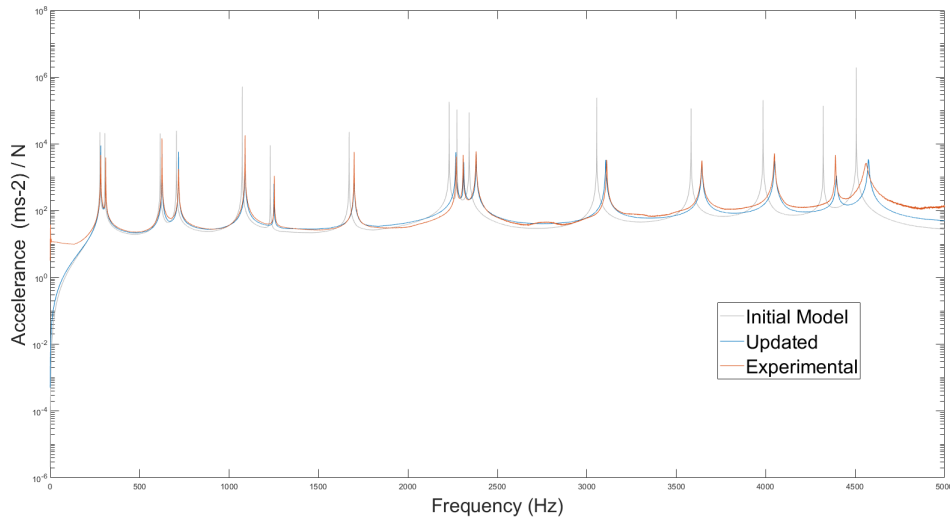


Figure 4.24: Rayleigh vs Modal Damping ratios per mode : A-Frame

#### 4.4.5 Updated Model



**Figure 4.25:** A-Frame SUM FRF : Updated vs. Initial vs. Experimental

Visually represented by figure 4.25 the comparison of the updated model FRF against experimental is shown. The correlation measured by the FRAC value is then increased to 0.9808 (up from the initial 0.9391).

Mode	Updated	Measurements	Delta	%
1	281.66	282.23	-0.57	-0.20%
2	309.837	310.49	-0.65	-0.21%
3	621.713	624.78	-3.07	-0.49%
4	715.685	717.36	-1.68	-0.23%
5	1086.68	1089.01	-2.33	-0.21%
6	1244.84	1252.54	-7.70	-0.61%
7	1691.84	1698.70	-6.86	-0.40%
8	2260.1	2269.02	-8.92	-0.39%
9	2304.22	2308.68	-4.46	-0.19%
10	2372	2380.50	-8.50	-0.36%
11	3094.18	3111.12	-16.94	-0.54%
12	3632.08	3642.74	-10.66	-0.29%
13	4033.14	4048.08	-14.94	-0.37%
14	4372.66	4389.76	-17.10	-0.39%
15	4566.51	4559.54	6.97	0.15%

**Table 4.7:** Updated vs Experimental Eigenfrequencies : A-Frame

After model updating, taking the mean square error for the eigenfrequencies seen in table 4.7 is also reduced down to 35.51 (from the original 155.46 with the initial model).

The range of the percentage errors to the frequencies are also visibly within the range of consistently less than 0.54%. Significantly reduced from the maximum of 1.79% in the initial model.

#### 4.4.6 MAC

For comparison figure 4.26 shows the MAC for the experimentally obtained eigenmodes against themselves while the figure 4.27 shows the MAC between the experimentally obtained eigenmodes and those of the updated model. The correlation between the eigenmodes is almost identical as visible through the values close to 1 along the diagonal.

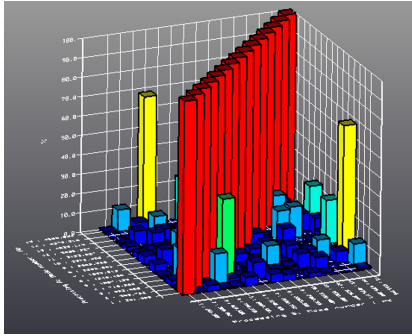


**Figure 4.26:** Experimental MAC : A-Frame

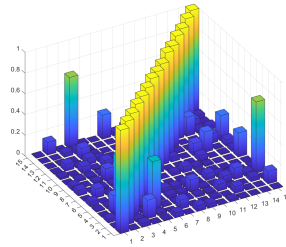


**Figure 4.27:** Experimental vs. Numerical MAC : A-Frame

Similar characteristics can also be seen between the differing eigenmodes for the values that do not lie on the diagonal for example where the modes 4 and 15 have moderate correlation values.

## 4.5 Model Updating Case: Beam

### 4.5.1 Initial Model Results

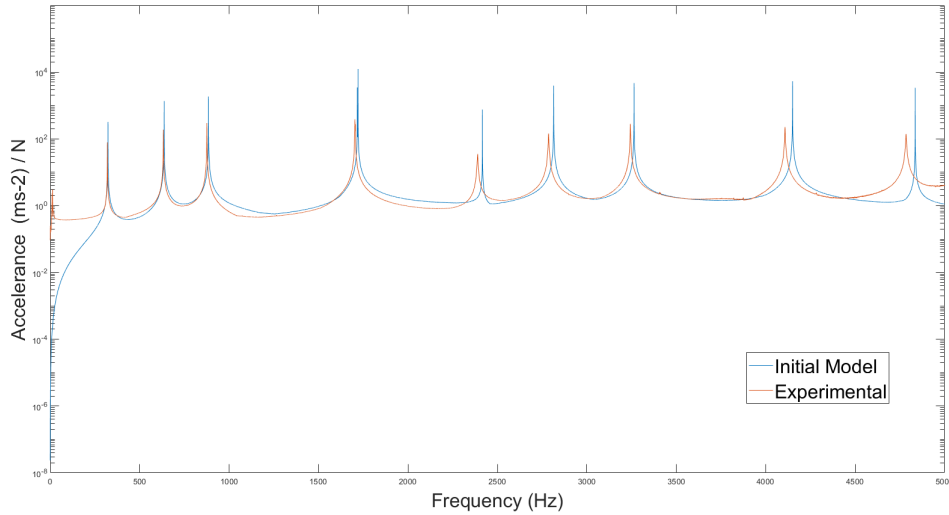


**Figure 4.28:** Beam SUM FRF : Initial vs. Experimental

Here in figure 4.28, the sum of the FRFs for the beam structure experimentally with the less-invasive configuration (1 accelerometer) and the initial numerical model are presented together. A FRAC value of 0.8736 is obtained. Similarly to the A-Frame, there is loss in correlation relating to the exclusion of both boundary conditions and rigid body modes in the numerical model. With all input projected onto the first 10 eigenmodes, there is no response as the input approaches 0 Hz in frequency.

Mode	Initial	Measurements	Delta	%
1	322.70	319.42	3.28	1.03%
2	636.71	632.41	4.30	0.68%
3	884.80	875.67	9.13	1.04%
4	1716.60	1703.15	13.45	0.79%
5	1720.74	1705.69	15.05	0.88%
6	2416.28	2389.17	27.11	1.13%
7	2814.45	2785.91	28.54	1.02%
8	3263.80	3243.50	20.30	0.63%
9	4150.06	4107.72	42.34	1.03%
10	4835.77	4784.18	51.59	1.08%

**Table 4.8:** Initial vs Experimental Eigenfrequencies : Beam

Taking the mean square error of the eigenfrequencies of table 4.8 for the initial model is 83.28. The range of percentage errors is consistent between 0.5% to 1.1%. Likely indicating too high stiffness (Youngs modulus value) or alternatively a lack of mass and a lower density value needed to represent the structure.

### 4.5.2 Updated Density

With a weight measurement of the beam at 1.791kg, for the given dimensions we calculate the density to be 7.749 kg/m<sup>3</sup>.

Initial Density: 7800kg/m<sup>3</sup> -> 7749kg/m<sup>3</sup> Updated

### 4.5.3 Parameter Optimisation

After the matlab optimisation through levenbourg marquardt algorithm, we obtain the following updated parameters:

Initial Youngs Modulus: 210,000 MPa -> 203,393 MPA Updated

Initial Poisson Ratio: 0.27 -> 0.259 Updated

### 4.5.4 Damping Comparison

Rayleigh damping was implemented with values calculated through a least squares approach against the experimentally obtained damping ratios per mode. The obtained  $\alpha$  and  $\beta$  parameters were:

$$\alpha = 1.4147$$

$$\beta = 2.5352E^{-8}$$

The effective damping ratio per mode is plotted in figure 4.29 below, showing the difference between Rayleigh damping scheme the measured damping ratios.

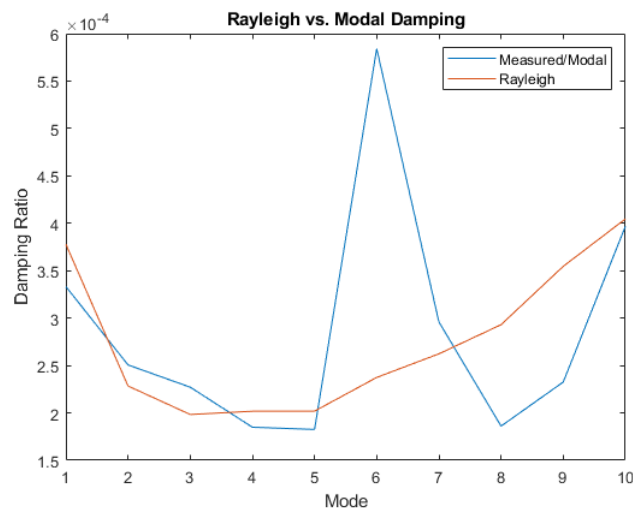
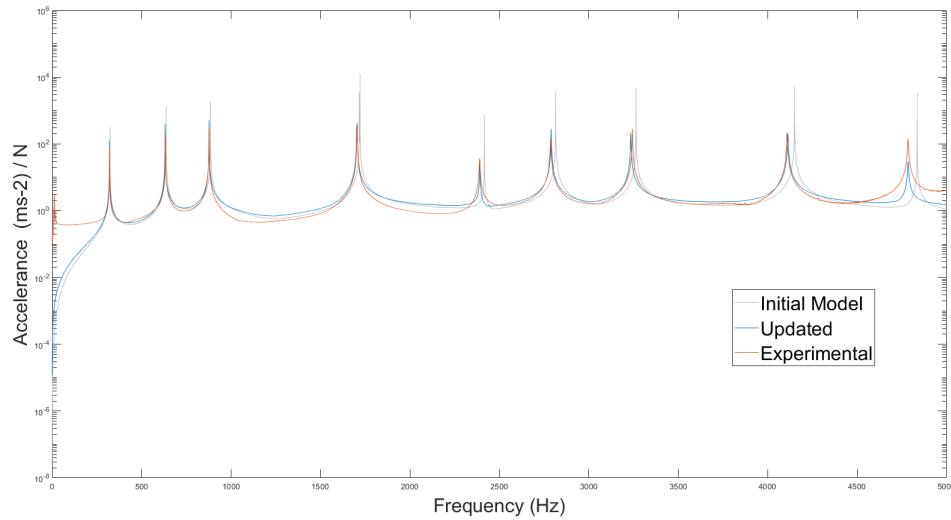


Figure 4.29: Rayleigh vs Modal Damping ratios per mode : Beam

### 4.5.5 Updated Model



**Figure 4.30:** Beam Sum FRF Updated vs Initial vs Experimental : Beam

Comparing the FRFs as seen in figure 4.30, after implementation of the model updating workflow the FRAC value is then increased to 0.9005 (up from the initial 0.8736).

Mode	Updated	Measurements	Delta	%
1	319.81	319.42	0.39	0.12%
2	630.99	632.41	-1.42	-0.22%
3	876.87	875.67	1.20	0.14%
4	1701.13	1703.15	-2.02	-0.12%
5	1705.30	1705.69	-0.39	-0.02%
6	2390.75	2389.17	1.58	0.07%
7	2789.17	2785.91	3.26	0.12%
8	3234.23	3243.50	-9.27	-0.29%
9	4112.73	4107.72	5.01	0.12%
10	4784.71	4784.18	0.53	0.01%

**Table 4.9:** Updated vs Experimental Eigenfrequencies : Beam

After updating the parameters the mean square error of eigenfrequencies in table 4.9 is reduced down to 11.50 (from the original 83.28 with the initial model).

The range of the percentage errors to the frequencies are also visibly within the range of consistently less than 0.3%. Significantly reduced from the maximum of 1.13% in the initial model.

## 4.5.6 MAC

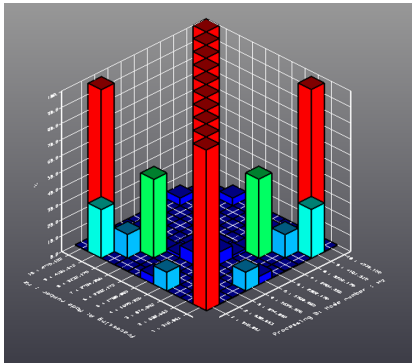


Figure 4.31: Experimental MAC : Beam

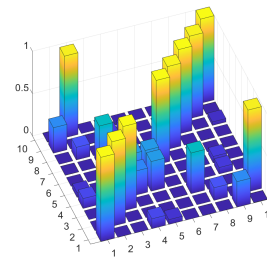


Figure 4.32: Experimental vs Numerical MAC : Beam

Figure 4.31 shows MAC for the experimental eigenmodes shapes with themselves, strong correlation value can be seen for eigenmode 2 and 10. This is a discretisation issue further explored in the discussion section.

The beam structure has its 4th and 5th eigenmodes very close in terms of frequency. While the updating workflow has reduced overall eigenfrequency error, it is visible from the MAC in figure 4.32 that there is not strong correlation between the 4th and 5th eigenmode shapes when comparing the experimental modes to that of the updated numerical model eigenmodes.

When comparing the beam structure eigenmode shapes visually in the appendix A.1, it is clear that the 4th and 5th eigenmodes of the experimental results are the 5th and 4th eigenmodes of the numerical model respectively.

In addition the sensitivity study shows that further changes to either the Youngs modulus or Poisson ratio will not have individual effects to the 4th or 5th modes. This highlights an issue with the updating workflow defined in this paper - it hints towards a likely need of further parameters for updating, see the following discussion sections.

## 4.6 Discussion

### 4.6.1 Experimental MAC Discretisation

Looking to the validation of the eigenmode orthogonality we observe some pairs of different modes with large correlation values, where ideally they would be 0 for orthogonal modes. However it can be attributed to the lack of degrees of freedom used in the MAC.

For the beam structure we observe strong correlation between the 2nd mode and the 10th mode. Referring to the eigenmode shapes visually (See appendix A.1), it is observable as to why there is large correlation. The MAC comparison only considers the degrees of freedom at the location of the 5 accelerometers positions, as well as only translational displacements, as opposed to rotation which is present in the torsional modes.

Overall there is a lack of information included over the whole structure with the degrees of freedom used in the MAC and as a result the movements at these 5 positions happen to correlate well when taken in isolation, as seen in figures 4.34 and 4.35

Had more positions been able to be captured and measured, the entire torsional shape of the 10th mode present in the eigenmode would be compared, while the 2nd mode would only have its in-plane deformation eigenmode shape. The MAC would then be able to discern between the mode shapes.

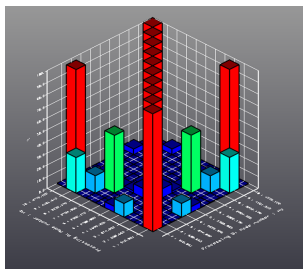


**Figure 4.33:** Experimental MAC : Beam

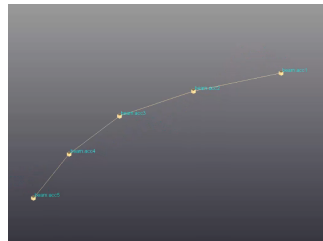


**Figure 4.34:** Mode 2: 632.41 Hz

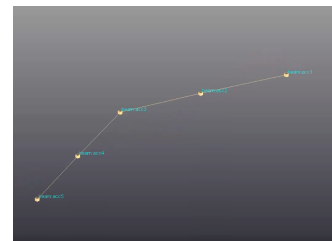


**Figure 4.35:** Mode 10: 4784.18 Hz

This similar effect is visible in that of the A-Frame where the 4th and 10th mode show moderate correlation. The correlation can be understood when the mode shapes are visually compared as in the appendix. A.2 Where there is a limited subset of the degrees of freedom compared then there is a larger correlation obtain as would be with the entire systems.

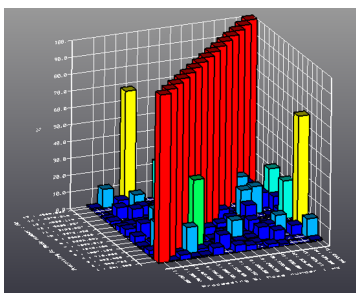


**Figure 4.36:** Experimental MAC : A-Frame

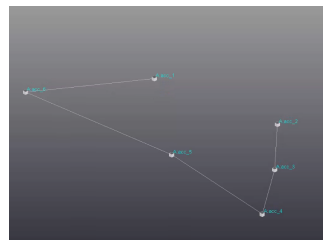


**Figure 4.37:** Mode 4: 717.36 Hz

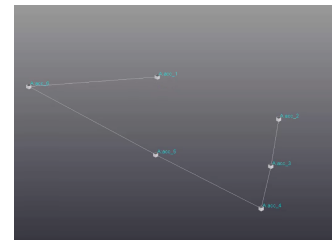


**Figure 4.38:** Mode 15: 4559.54 Hz

### 4.6.2 MAC - Experimental vs Numerical

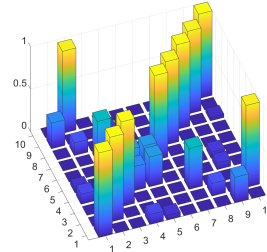
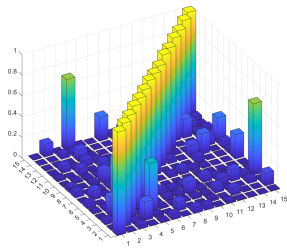


**Figure 4.39:** Experimental vs. Numerical MAC : A-Frame **Figure 4.40:** Experimental vs. Numerical MAC : Beam

Through use of the MAC between experimental eigenmodes against themselves and also against numerical eigenmodes, there is strong correlation for the A-Frame structure seen in figures 4.39 and 4.40.

When taking the entire eigenmodes obtained numerically, meaning all degrees of freedom, they are by their construction during the numerical eigensolver process orthogonal. Given the strong correlations of the MAC between the experimentally obtained and numerically obtained eigenmodes for the A-Frame, it is good indication that it is due to the limited degrees of freedom used in the MAC calculation.

For the Beam structure however there is little correlation shown in the MAC between the 4th and 5th eigenmodes seen in figure 4.40. Upon comparison of the eigenmode shapes seen in figures 4.41 to 4.44, it is understood why. This is due to the ordering of the modes is based on the eigenfrequency values, of which the 4th and 5th modes are very close. This issue is explored further in the following sections.

### 4.6.3 Modes with close Eigenfrequencies

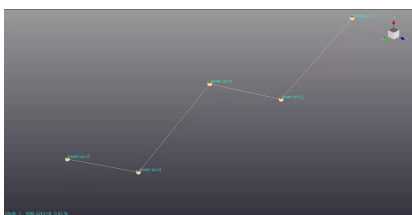


**Figure 4.41:** Experimental Mode 4

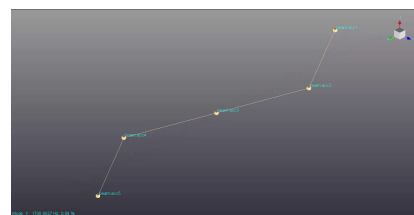


**Figure 4.42:** Experimental Mode 5

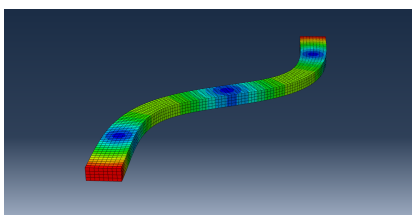


**Figure 4.43:** Numerical Mode 4

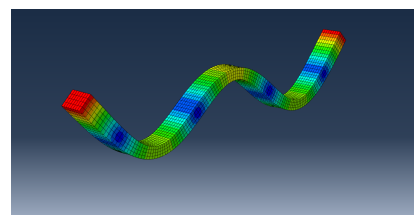


**Figure 4.44:** Numerical Mode 5

This highlights potential issues for the updating workflow in that the ordering of the abaqus modes are dependant on frequency. Updating with the aim to address the issue of the 4th and 5th modes can also cause inconsistent comparisons if the ordering of the eigenmodes are taken directly from abaqus.

There would be the requirement to have extra conditions that enforce that specific eigen-frequency differences which are being optimised for correctly correspond to the relevant eigenmodes. This could be potentially addressed through using the MAC included as some component of the objective function during the optimisation.

From the sensitivity study it is observed however the updating parameters of Youngs modulus and Poisson ratio affect the 4th and 5th modes somewhat consistently, that meaning that further iterations over these parameters are likely to not resolve the ordering of the eigenmodes either. This leads to the following section where potentially beam dimensions could be implemented in the model updating workflow.

#### 4.6.4 Beam - Structure Dimensions

The dimensions are regarded as parameters that can be taken as known since they are able to be measured. However there are always tolerances for error, depending on how the measurement is taken for example and where.

For instance the beam cross section measurements could be taken at one point and assumed to be constant across the length, which may not necessarily be the case. For this experiment, the cross-sectional profile measurements were taken at the 5 accelerator locations along the 50cm length of the beam.

Using these base values, they were varied by +/- 0.5 percent which is a conservative tolerance given the variance of the measurements taken at different points were significantly smaller.

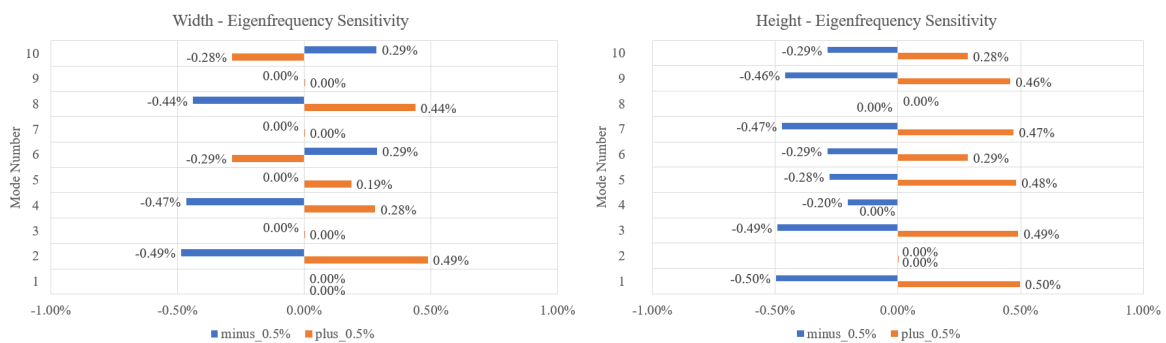


Figure 4.45: Beam Eigenfrequency Sensitivity to Width Figure 4.46: Beam Eigenfrequency Sensitivity to Height

Observable in figures 4.45 and 4.46 are the effects of the dimensions to the respective modes for the simple beam shape. A clear correlation between the plane of which the mode shape has most deformation is affected by the cross-sectional dimension that effects it ie. bending stiffness. Moreover is the relationship non-linear.

The digital measurement caliper used to obtain the dimensions is mentioned to have a accuracy of  $\pm 0.02\text{mm}$ .

The dimensions measured across the length of the beam are as follows:

	acc1	acc2	acc3	acc4	acc5
width	30.30	30.23	30.26	30.24	30.27
height	15.20	15.20	15.21	15.18	15.19

**Table 4.10:** Variance in profile dimensions along beam length

This overview is used to obtain an understanding of the potential upper and lower bounds in the case dimensions are included as the updating parameters. Given the sensitivity to specific sets of eigenfrequencies and the variance in measurements obtained, it shows benefit to be obtained in including them as updating parameters but only within bounds similar to those observed from measurement positions and the caliper accuracy.

However relating this to the previous section, an increase in the width and decrease in height would increase the eigenfrequency of 4th mode and reduce the eigenfrequency of the 5th mode in the numerical model and likely resolve the issue of the eigenmode ordering previously discussed.

This does not address the first step involving the weight calculation as part of the updating workflow to isolate and calculate the density parameter before optimisation. By changing dimensions during the optimisation iterations would invalidate this step as the density no longer applies to the changed geometry.

Although this presents a problem, there could be further modifications to the workflow to address this and opens an avenue for further model updating workflows to be explored.

#### 4.6.5 Measurement errors and assumptions

The model updating workflow relies upon the accuracy of several measurements and the discretisations involved. There are several sources of inaccuracy and errors that are introduced and in addition need to be addressed.

##### Weight measurement accuracy digit

The limited significant digits of the weight mean there is a corresponding loss of accuracy in the density value in its calculation over the volume.

##### Equipment accuracy

The measurement equipments each are utilised with knowledge of their own tolerances, an example is that of the dimensions which could perhaps be then included as part of the updating parameters to address this inaccuracy.

##### Testing errors/assumptions

Inherently there is also discrepancies between the ideal definitions in the numerical model to that of testing, specifically examples are hammer impact direction, accelerometer align-

ment, adhesive of the accelerometers of which could also be potential sources of error and differences.

#### FRF measurement discretisation

The interval discretisation of the frequencies obtained, greatly affect the obtained damping ratio as it is very sensitive to the peak shape and position. The damping ratio calculation interpolates between the measured points, introducing potential for error.

#### 4.6.6 Laser vs Accelerometer results

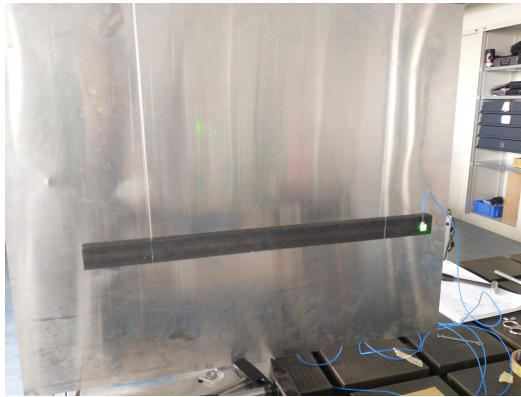


**Figure 4.47:** Laser and Accelerometer overlaid measurement

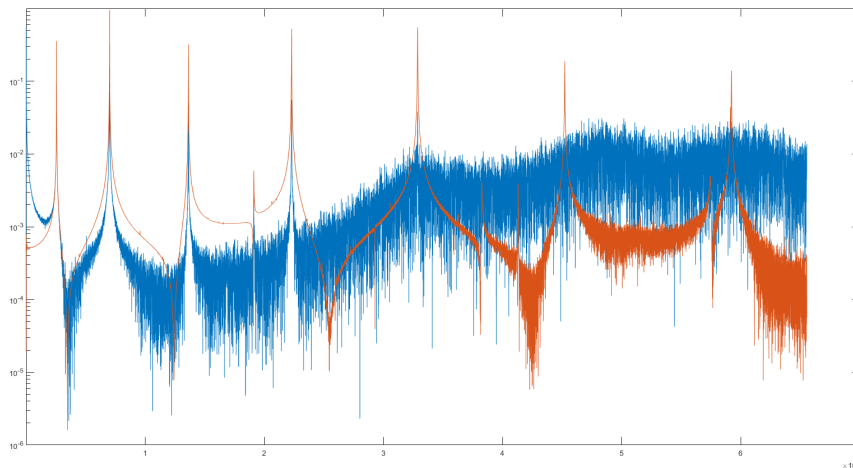


**Figure 4.48:** FRF response Laser (Blue) and Accelerometer (Orange)

in figure 4.48 we observe the FRFs from the accelerometer and the laser in the second configuration overlaid, the resulting difference of the 2 measurements could be observed. It should be noted the output values measured by the laser are velocity where as those from the accelerometers are acceleration.

The loss of clarity in the laser measurements is clear against that of the accelerometer. However the eigenfrequencies and damping values obtained as a result are consistent between the 2 measurements.

#### 4.6.7 Invasive testing influence on eigenfrequency

To explore the effect on the eigenfrequencies of the structures due to the additional mass from the accelerometers, a comparison is drawn between the experimentally obtained eigenfrequencies for the different number of accelerometers against the same configurations in the numerical model.

The weight of each accelerometer (2.3 grams) are added as point masses at the corresponding accelerometer locations within the numerical model. The magnitude of the percentage decreases are show for each mode frequency. This should have good agreement between the experimental and numerical results.

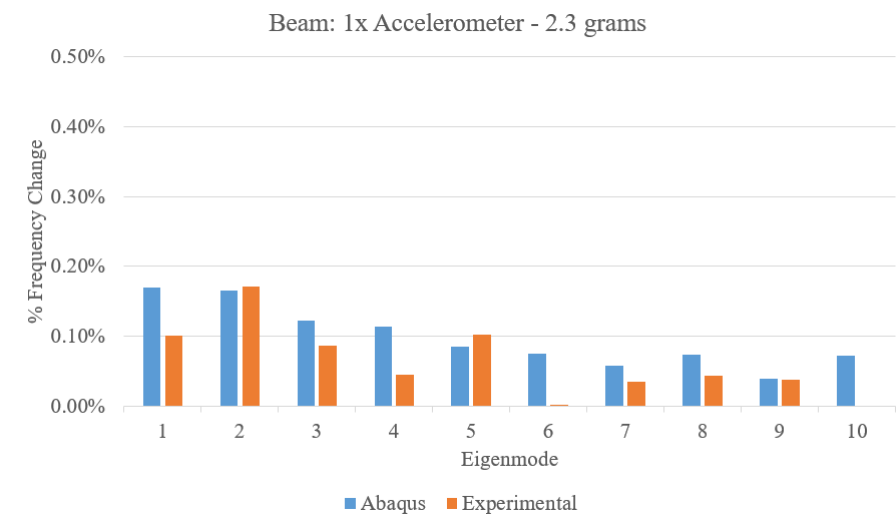


**Figure 4.49:** Beam Eigenfrequency sensitivity to 1 Accelerometer mass

Figures 4.49 and 4.50 represent the magnitudes of the frequency shifts of both configurations (1 accelerometer and 5 accelerometers) against the laser measurements where no mass is added to the beam structure. The graphs show reasonable correlation between the experimental and numerical models. While there exists variance in amplitudes of the values, they appear to have good agreement when looking at the averages.

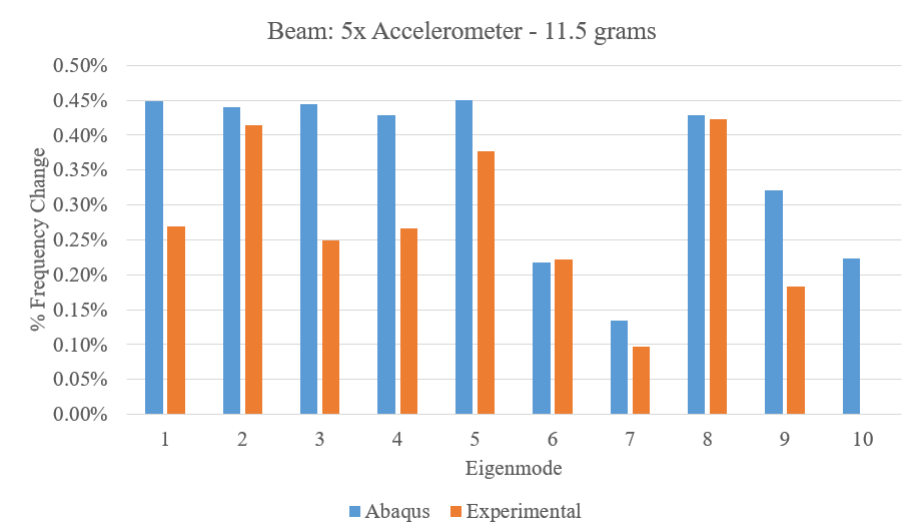


**Figure 4.50:** Beam Eigenfrequency sensitivity to 5 Accelerometer mass

Similarly the comparison is made on the A-Frame structure in figure 4.51, however for this case there was no measurement taken with the laser. Instead a comparison is made between the eigenfrequencies and how they change between having 2 accelerometers attached against 6 accelerometers. Observable is again good agreement between the experimental and numerical model configurations.

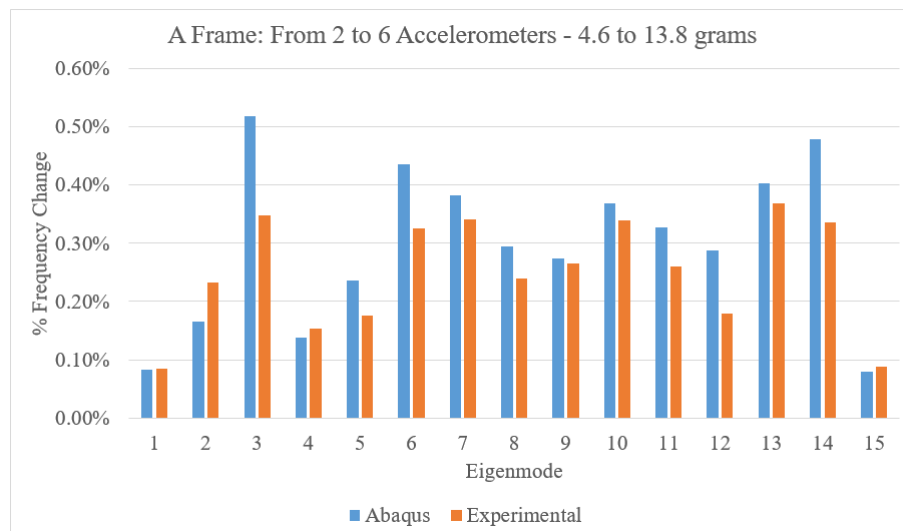


**Figure 4.51:** A-Frame Eigenfrequency Sensitivity from Accelerometer mass

Further note is the difficulty in measurement of the accelerometer weights as they were unable to be detached from the signal cables and as a result an average of several measured weights was taken. The variance was not so great yet still illustrates the potential difference in the experimental setup and the numerical model with a perfect point mass of 2.3 grams.

### 4.6.8 Invasive testing influence on damping

Significant additional damping was measured in the structure with more invasiveness in the measurement configuration. The following figures 4.52 and 4.53 present the calculated damping ratios from the Siemens software for each mode and each configuration.

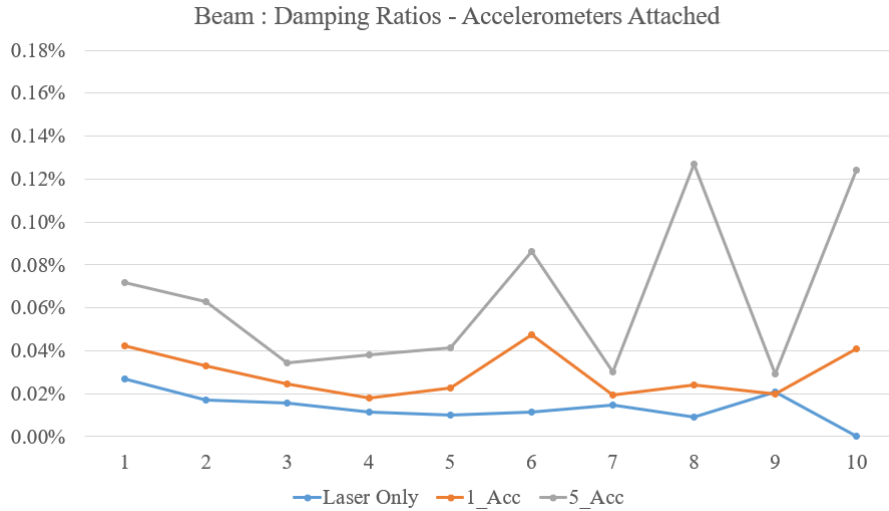


Figure 4.52: Beam Damping Sensitivity to Accelerometers

Without the attached accelerometers to the structure there was significantly lower damping ratios obtained, with the addition of a single accelerometer there was significant increase in the damping. With all 5 accelerometers there were even larger damping ratios obtained. This phenomenon was consistent between both the beam and A-frame structure and can likely be attributed to the energy lost through the accelerometer signal cables as each structure was resonating.

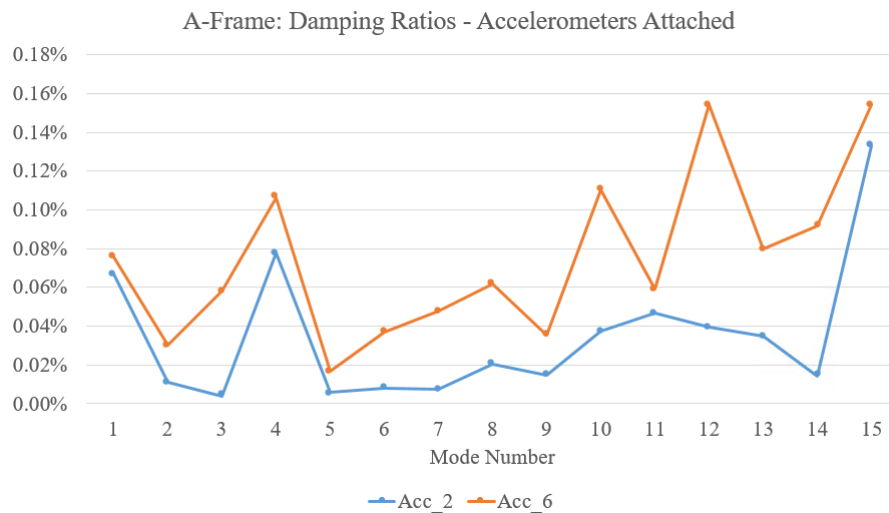


Figure 4.53: A-Frame Damping Sensitivity to Accelerometers

### 4.6.9 Damping Scheme Comparison

#### Modal Damping

The modal damping scheme is able to be applied with the exact desired damping ratios applied across each individual eigenmode used to represent the system. Using this allows direct input of the experimentally obtained damping ratios into the numerical model as damping per mode. This immediately presents the problem however where the damping of higher modes not solved for is important in the real system response. In addition it does not present a general damping matrix which could be used for a direct method solution to the system, it is useful only when using modal superposition.

#### Structural Damping

Structural Damping, while provides a damping ratio that is independent of frequency, solving the potential issue from modal damping, however is only able to be implemented for steady state excitation and also only allows consistent damping which may not accurately represent the system.

#### Rayleigh Damping

Rayleigh damping provides a viscous damping matrix capable of being implemented for both steady state harmonic analyses but also solving for direct solutions done iteratively without modal superposition, presenting the most ideal damping scheme and therefore is used in the model updating workflow explored.

As the structures used in the workflow have very low damping ratios (approaching 0.05%), the damping can be considered irrelevant to the eigenfrequencies since the resulting shift is very small. This results in the method used in the paper being least squares to reduce the error of the effective rayleigh damping against measured modal damping ratios. It can also include as many damping ratios as there are modes measured and included in the modal testing FRF results.

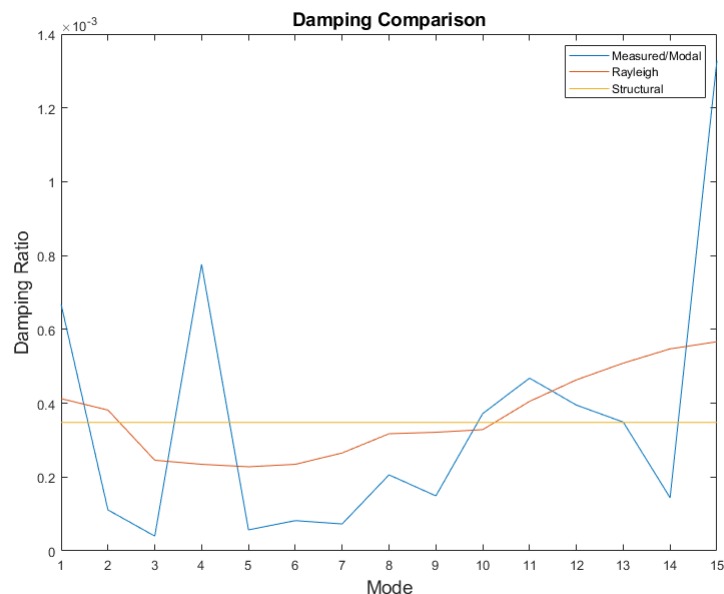
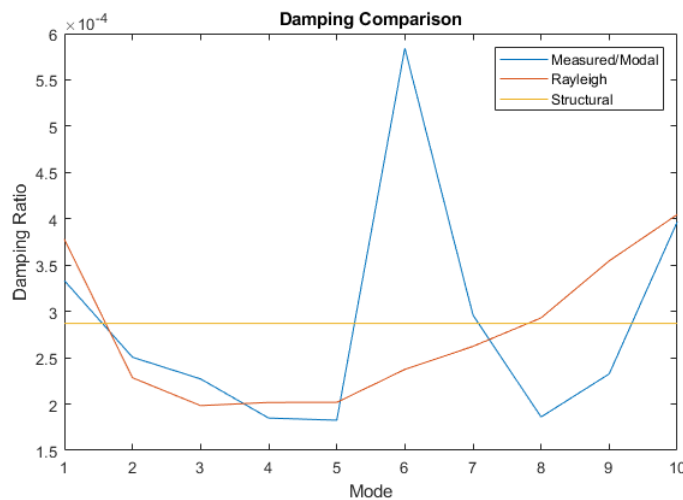


Figure 4.54: Damping Ratios for Damping Schemes : A-Frame

So in terms of applicability the Rayleigh damping scheme presents itself as the robust and useful. In terms of the FRF correlation, each damping scheme has not such a large effect in these structures as the damping ratios themselves are very small. There is almost no visible difference in the FRFs with different damping schemes excepting small changes in the resonance peak heights.

For comparison in terms of FRF correlation, the values of the FRAC for each of the damping schemes for the A-Frame structure are:

Modal - 0.9001  
 Rayleigh - 0.9808  
 Structural - 0.9709



**Figure 4.55:** Damping Ratios for Damping Schemes : Beam

Similarly for the A-Frame structure the FRAC correlation values against the experimental results change depending on the damping scheme as so:

Modal - 0.9004  
 Rayleigh - 0.9005  
 Structural - 0.9006

For the case where damping ratios are larger or if the damping behaviour of specific components in an assembly was of interest, a different approach could be used where the damping parameters, whether Rayleigh constants or Structural damping factor for individual structures, could be included in the sensitivity based iterations.

Such a case would involve using the FRAC and the correlation of the numerical FRF against experimental FRF as the objective function to minimise.

### 4.6.10 Beam - Configuration comparison

While the damping ratios obtained through the Siemens software were used as the reference in the model updating method, the calculation of damping ratios was quite sensitive to both the method used in calculating as well as the configuration of the structure.

The two calculation methods for the damping ratios compared are that used by the Siemens software and separately obtained ratios using the 3db method in a matlab script. In addition comparison between using the sum FRF's for each strike position as well as the individual FRFs for each relevant strike position.

The figures below 4.56 and 4.57 illustrate the variance in the damping ratios as a result (ideally each curve should be the same as each other). The two configurations C1 and C2 are short for config 1 and config 2 as illustrated in appendix item A.4.

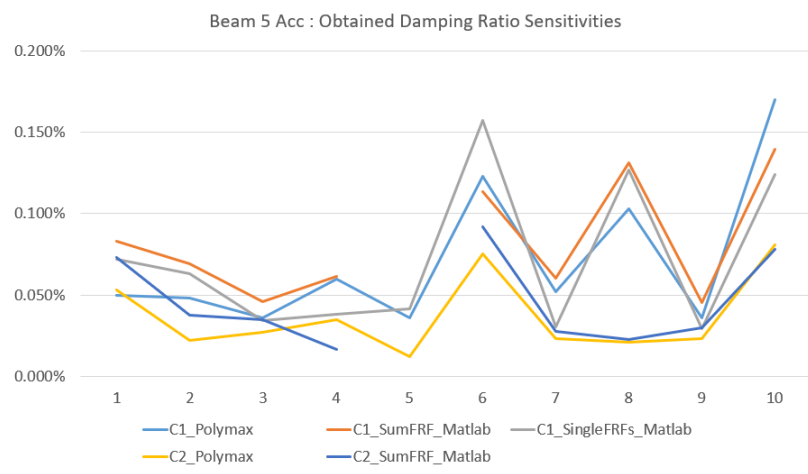


**Figure 4.56:** Variance In Measured Damping Ratios - Beam 5 Accelerometers

There is also variance present in the damping ratios when 1 accelerometer is used, however visibly less than that of when 5 accelerometers are used.

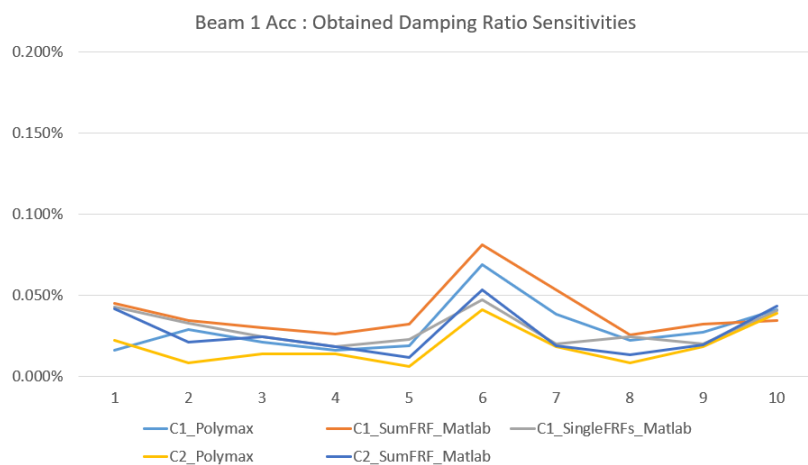


**Figure 4.57:** Variance In Measured Damping Ratios - Beam 1 Accelerometer

#### 4.6.11 Model Updating Effectiveness

As an overview we see the improvement over several dynamic outputs from the numerical model against experimental data in the following table. The squared errors from the eigenfrequencies themselves are reduced from 83.28 to 11.50 for the beam and from 155.46 down to 35.51 for the A-Frame.

The beam structure presented however the problem regarding the eigenmode ordering for specific cases where there are eigenmodes with similar eigenfrequencies. For confidence in the updating method this issue must be addressed and compensated for during the optimisation procedure.

While the Rayleigh damping scheme proved most generally applicable, the question still maintains of what to be used as reference damping values. The Rayleigh damping curve tends to characterise the measure damping ratios well yet there is still large variance depending on the measurement configuration and accelerometers used. In summary that damping remains a large unknown and is more relevant to the boundary conditions as opposed to the structure itself.

The FRAC criterion represents a value that reflects the overall agreement between measurement results and those obtained numerically. As it correlates shapes of the FRF, it automatically includes correlation between both the eigenfrequencies obtained as well as the damping ratios. Through the model updating workflow defined in the paper, the FRAC values are observed to increase from 0.8736 to 0.9005 for the Beam and up to 0.9808 from 0.9391 for the A-Frame structures.



## Chapter 5

### Conclusion

The paper explores a model updating workflow able to be implemented for single structures of consistent, homogenous material. Through implementing the defined workflow, the density of the structure is able to be calculated and isolated from the optimisation step, improving the definition of the non-linear problem. The remaining unknown parameters of Youngs Modulus and Poisson Ratio are optimised through a sensitivity based updating scheme, preserving the physical relevance of the model [5].

The Damping schemes of Rayleigh, Structural and Modal and their applicability were compared. The parameters of the schemes directly implemented or calculated through a least-squares approach against experimental damping ratios. Observed errors between experimentally obtained dynamic outputs are reduced in terms of both the eigenfrequencies and also an improved overall response characterised by correlation in the FRAC.

The Beam structure presented a case with eigenmodes of similar eigenfrequencies, affecting the order of the eigenmodes used in optimisation step. In such cases the model updating method must be modified to explore and include further updating parameters, namely dimensions were observed to be potential parameters to compensate for measurement tolerances and improve this error.

The results have illustrated the effect of measurement invasiveness has on the dynamic outputs of the structure specifically from the added mass of accelerometers and also the damping observed from the wires from accelerometers and also wires and structure positioning in aiming to achieve free-free boundary conditions.

The least invasive configuration using the laser only presented the least amount of damping observed and did not cause a shift in eigenfrequencies. The question then remains to what degree is the remaining damping due to the wires providing the boundary conditions compared to other ways energy is lost through internal material friction, air resistance and sound.

What can be taken from these results is a workflow to obtaining a validated numerical model for a single structure in terms of the linear mass and stiffness properties. These single structures can then be confidently used in assembly configurations where then the more complex topics of contact, friction, pre-tension can be independantly and further explored.

As observed in this paper the damping observed in the single structure is already heavily dependant on the measurement setup and its invasiveness, leaving a small, yet difficult to determine proportion of the damping due to the energy lost within the structure itself.

## 5.1 Further exploration

Damping parameters in this example were obtained using direct calculation of least squares to have the best fitting parameters and was possible since they were considered independent from eigenfrequencies of the system. However in assemblies or structures of other materials it is not likely the case, in which the damping parameters must be modified iteratively against an objective function, for example the system FRFs, which then encapsulates both the eigenfrequencies and damping response of the system.

Further exploration of the model updating method is to compare results in other forms to have more complete understanding of the updating validity. Such an example could be the raw force signal from testing and perform direct solutions in the numerical model to further validate updated parameters.

This would however involve similar issues regarding choice of boundary condition and the ability to isolate the structure. However it is of particular interest where higher eigenfrequency inputs are explored, as the updated parameters of both young's modulus and damping are then still applicable when solving the system directly, despite only previously having used the dynamic response up to measurable frequencies of the modal impact testing 5000Hz for the updating procedure.

Additionally further testing with various free-free boundary conditions ie. wires at different positions that maybe obstruct a different set of eigenmodes, different wire types. This could provide the benefit of a more comprehensive picture on the observed damping in the system as a result.

Additional accelerometers could too provide benefit in having more confidence in the MAC criterion. Despite the change in observed damping and eigenfrequency shift with additional accelerometers, this would better represent the entire structure with more degrees of freedom and ideally approach consistent orthogonality between eigenmode shapes.

Another option could be to implement combined Rayleigh and Structural damping in unison for cases of steady state analysis to search out better damping improvement.

# Appendix A

## Appendix

### A.1 Beam Eigenmodes

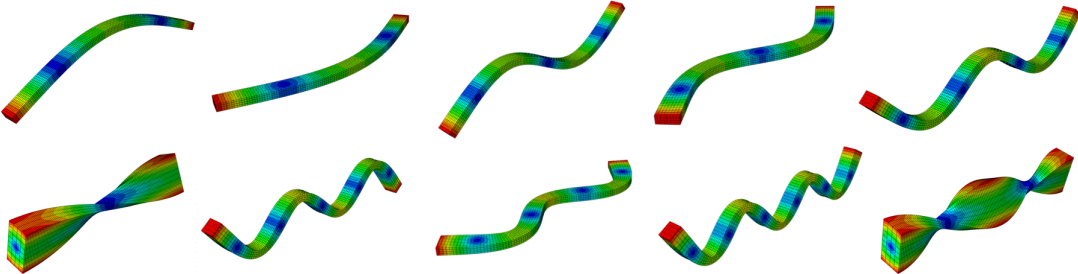


Figure A.1: Numerical Model First 10 Eigenmodes (Sequential order): Beam .

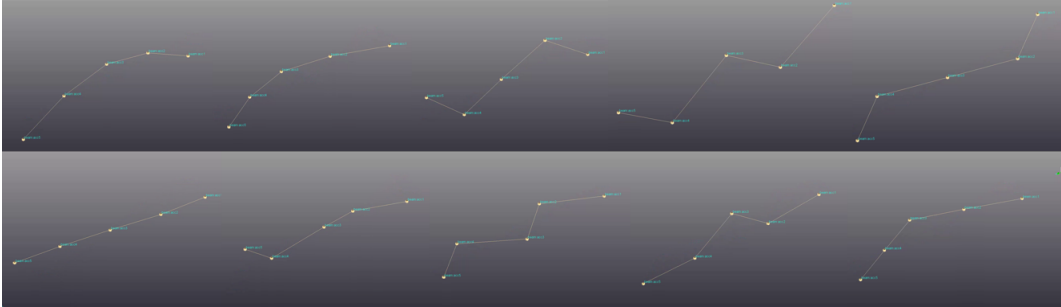
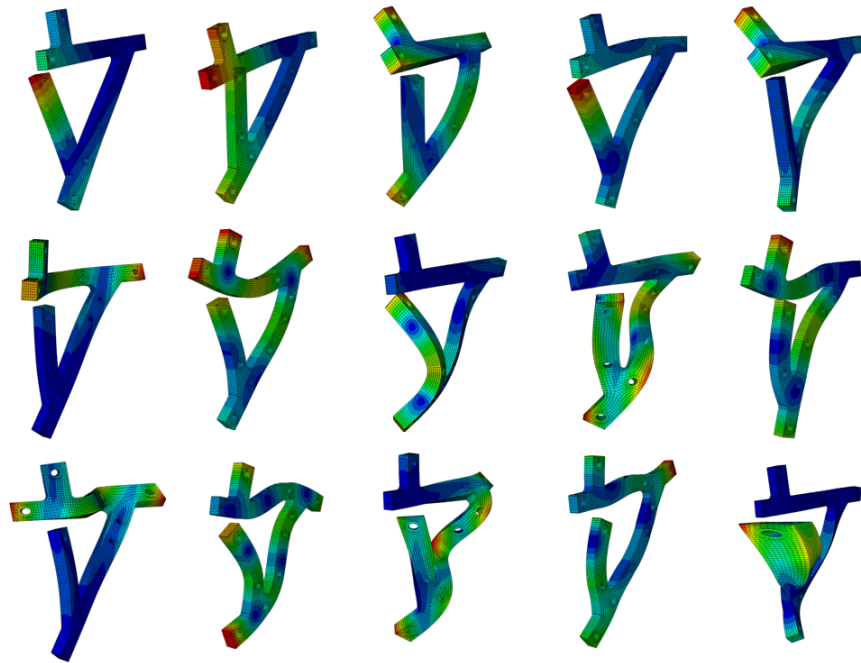


Figure A.2: Experimental Model First 10 Eigenmodes (Sequential order): Beam .

## A.2 A-Frame Eigenmodes



**Figure A.3:** Numerical Model First 15 Eigenmodes (Sequential order): A-Frame .



**Figure A.4:** Experimental Model First 15 Eigenmodes (Sequential order): A-Frame.

### A.3 A-Frame MAC Table

	1	2	3	4	5	6	7	8	9	10	11	12	13	14	15
1	100.0	0.5	3.0	0.8	0.9	4.5	0.1	4.3	3.2	0.4	2.2	1.2	0.0	0.5	0.9
2	0.5	100.0	1.9	16.3	2.4	0.0	9.0	0.1	0.2	1.7	0.1	7.2	0.5	0.2	11.3
3	3.0	1.9	100.0	1.6	41.3	1.0	1.7	0.8	1.3	2.2	7.7	2.1	0.2	6.1	0.6
4	0.8	16.3	1.6	100.0	2.6	0.0	2.3	2.3	11.2	1.5	0.5	6.2	10.7	3.5	67.8
5	0.9	2.4	41.3	2.6	100.0	0.3	6.7	2.4	2.2	0.7	7.4	4.7	0.4	0.0	1.6
6	4.5	0.0	1.0	0.0	0.3	100.0	0.0	0.1	0.2	0.7	1.4	1.0	0.0	0.3	0.0
7	0.1	9.0	1.7	2.3	6.7	0.0	100.0	0.0	2.9	5.2	2.6	1.3	0.0	0.0	22.5
8	4.3	0.1	0.8	2.3	2.4	0.1	0.0	100.0	0.3	0.1	0.0	8.4	0.3	1.0	3.4
9	3.2	0.2	1.3	11.2	2.2	0.2	2.9	0.3	100.0	5.4	0.0	15.2	16.4	0.4	8.8
10	0.4	1.7	2.2	1.5	0.7	0.7	5.2	0.1	5.4	100.0	1.0	0.2	0.5	9.4	23.0
11	2.2	0.1	7.7	0.5	7.4	1.4	2.6	0.0	0.0	1.0	100.0	0.0	0.2	4.5	0.6
12	1.2	7.2	2.1	6.2	4.7	1.0	1.3	8.4	15.2	0.2	0.0	100.0	15.4	2.7	3.0
13	0.0	0.5	0.2	10.7	0.4	0.0	0.0	0.3	16.4	0.5	0.2	15.4	100.0	8.6	2.5
14	0.5	0.2	6.1	3.5	0.0	0.3	0.0	1.0	0.4	9.4	4.5	2.7	8.6	100.0	2.9
15	0.9	11.3	0.6	67.8	1.6	0.0	22.5	3.4	8.8	23.0	0.6	3.0	2.5	2.9	100.0

**Table A.1:** Experimental MAC Numerical Values : A-Frame

### A.4 Beam Configuration Positions

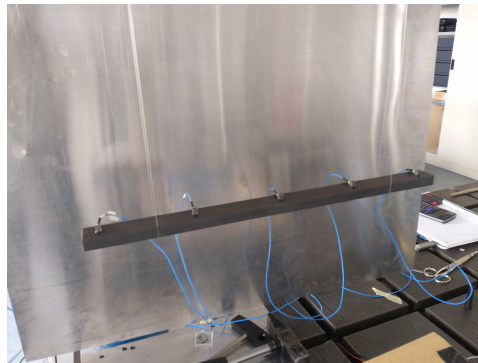


**Figure A.5:** Beam Configuration 1.



**Figure A.6:** Beam Configuration 2.



## Bibliography

- [1] Allemang, R. “The Modal Assurance Criterion (MAC): Twenty Years of Use and Abuse”. In: *Sound and Vibration* 37 (Jan. 2003).
- [2] Burkhart, T., Andrews, D., and Dunning, C. “Finite element modeling mesh quality, energy balance and validation methods: A review with recommendations associated with the modeling of bone tissue”. In: *Journal of biomechanics* 46 (Apr. 2013). DOI: 10.1016/j.jbiomech.2013.03.022.
- [3] Cardarelli, F. *Materials Handbook: A Concise Desktop Reference*. Springer London, 2008. ISBN: 9781846286698. URL: <https://books.google.de/books?id=PvU-qbQJq7IC>.
- [4] Cheung, Y. and Leung, A. *Finite Element Methods in Dynamics*. Solid mechanics and its applications. Springer Netherlands, 1992. ISBN: 9780792313137. URL: <https://books.google.de/books?id=l67Afd4ga4gC>.
- [5] Friswell, M. and Mottershead, J. *Finite Element Model Updating in Structural Dynamics*. Solid Mechanics and Its Applications. Springer Netherlands, 1995. ISBN: 9780792334316. URL: <https://books.google.de/books?id=KyMVKqrEEZIC>.
- [6] Gavin, H. P. “The Levenberg-Marquardt method for nonlinear least squares curve-fitting problems c ©”. In: 2013.
- [7] Grafe, H. *Model Updating of Large Structural Dynamics Models Using Measured Response Functions*. University of London, 1998.
- [8] Kelley, C. *Iterative Methods for Optimization*. Frontiers in Applied Mathematics. SIAM, 1999. ISBN: 9781611970920. URL: <https://books.google.de/books?id=7oqAh1MAZG0C>.
- [9] Lu, Y. and Tu, Z. “A two-level neural network approach for dynamic FE model updating including damping”. In: *Journal of Sound and Vibration* 275.3 (2004), pp. 931–952.
- [10] M. Höser M. Böswald, Y. G. *Validating Global Structural Damping Models for Dynamic Analyses*. Deutscher Luft- und Raumfahrtkongress, 2015.
- [11] Otsuki, Y., Lander, P., Dong, X., and Wang, Y. “Formulation and application of SMU: An open-source MATLAB package for structural model updating”. In: *Advances in Structural Engineering* 25.4 (2022), pp. 698–715.
- [12] Qu, Z. *Model Order Reduction Techniques with Applications in Finite Element Analysis: With Applications in Finite Element Analysis*. Springer, 2004. ISBN: 9781852338077. URL: <https://books.google.de/books?id=Uo7wVEbbg2IC>.
- [13] Rixen, D. *Dynamics of Structures*. Technical University of Munich, Chair of Applied Mechanics, 2021.
- [14] Schmitz, T. and Smith, K. *Mechanical Vibrations: Modeling and Measurement*. Springer New York, 2011. ISBN: 9781461404606. URL: <https://books.google.de/books?id=fbyCcHPI0nsC>.



## Disclaimer

I hereby declare that this thesis is entirely the result of my own work except where otherwise indicated. I have only used the resources given in the list of references.

Garching, April 30, 2022

---

(Signature)